

Use of the ocean surface wind direction signal in microwave radiance assimilation

Masahiro Kazumori^{a*} and Stephen J. English^b

^a*Japan Meteorological Agency, Tokyo, Japan*

^b*European Centre for Medium-Range Weather Forecasts, Reading, UK*

*Correspondence to: M. Kazumori, 1-3-4 Otemachi, Chiyoda-ku, Tokyo 100-8122, Japan.
E-mail: kazumori@met.kishou.go.jp

We developed an empirical relative wind direction (RWD) model function to represent azimuthal variations of oceanic microwave radiances of vertical and horizontal polarizations. The RWD model function was based on radiance measurements from the Advanced Microwave Scanning Radiometer and Special Sensor Microwave Imager/Sounder (SSMIS). Ocean surface wind vector data from SeaWinds on board the Advanced Earth Observing Satellite-II and European Centre for Medium-range Weather Forecasts (ECMWF) Integrated Forecasting System were utilized for the RWD model function development. The RWD model function was introduced to a microwave ocean emissivity model: a FAST microwave Emissivity Model (FASTEM) in a radiative transfer model for satellite radiance assimilation. Performances of the RWD model function were much more realistic than present azimuthal model functions in FASTEM for low wind speed and high-frequency channels. Assimilation experiments using the RWD model function were performed in the ECMWF system. The experiment demonstrated reductions of first-guess departure biases arising from modelling of the azimuthal variations in areas of high wind-speed and low variability of wind direction. For example, bias reductions in ascending and descending SSMIS 19 GHz vertically polarized radiance in the Somali jet over the Arabian Sea were approximately 0.6 and 0.7 K. The bias reductions were found for all assimilated microwave imager channels in a wide wind-speed range. Moreover, analysis increments of specific humidity in the lower troposphere were reduced (e.g. 0.2 g kg⁻¹ reduction at 1000 hPa in the Somali jet). We found improvements of relative humidity and temperature in short-range forecasts in the lower troposphere. The experiment results clearly showed the importance of modelling the azimuthal variation of emissivity for assimilation of microwave imager observations. The new RWD model function, combined with the other components of FASTEM, will be available as FASTEM-6.

Key Words: ocean surface; emissivity; wind direction; azimuth angle; microwave imager; AMSR; radiance assimilation; numerical weather prediction

Received 14 January 2014; Revised 15 June 2014; Accepted 1 September 2014; Published online in Wiley Online Library

1. Introduction

Microwave radiance data measured from satellites is a crucial data source in data assimilation for numerical weather prediction (NWP). The radiance data are assimilated as brightness temperatures by means of radiative transfer calculations. Oceanic microwave radiance data contain various kinds of geophysical information: water vapour, atmospheric hydrometeors and ocean surface conditions. The sensitivity needs to be included in the radiative transfer calculations in order to make consistent changes in the initial state.

The ocean surface properties can be represented with a small number of parameters because the ocean surface is more

homogeneous than the land surface. For calm oceans, ocean surface emissivity can be accurately computed using the Fresnel equation by assuming a specular surface. The emissivity is expressed as a function of permittivity, sea-surface temperature and incidence angle. In practice, the ocean surface is rough. The primary cause of the surface roughness is wind. The ocean surface roughness increases the emissivity. Accurate modelling of the ocean surface emissivity is necessary in physically based remote sensing both for geophysical parameter retrievals, and in data assimilation.

Furthermore, the ocean surface radiance observed with microwave radiometers has a wind direction signal. The definition of the azimuth angle in this study and relevant angle information

Table 1. Microwave imager channel frequency.

Band	Notation	Polarization	Sensor (channel number and frequency (GHz))					
			AMSR-E		TMI		SSMIS	
			Ch	Frequency (GHz)	Ch	Frequency (GHz)	Ch	Frequency (GHz)
C	06V	V	1	6.925	—	—	—	—
	06H	H	2	6.925	—	—	—	—
X	10V	V	3	10.65	1	10.65	—	—
	10H	H	4	10.65	2	10.65	—	—
Ku	19V	V	5	18.7	3	19.35	13	19.35
	19H	H	6	18.7	4	19.35	12	19.35
K	23V	V	7	23.8	5	21.3	14	22.235
	23H	H	8	23.8	—	—	—	—
Ka	37V	V	9	36.5	6	37	16	37
	37H	H	10	36.5	7	37	15	37
W	89V	V	11	89.0A	8	85.5	17	91.655
	89H	H	12	89.0A	9	85.5	18	91.655
	—	V	13	89.0B	—	—	—	—
	—	H	14	89.0B	—	—	—	—

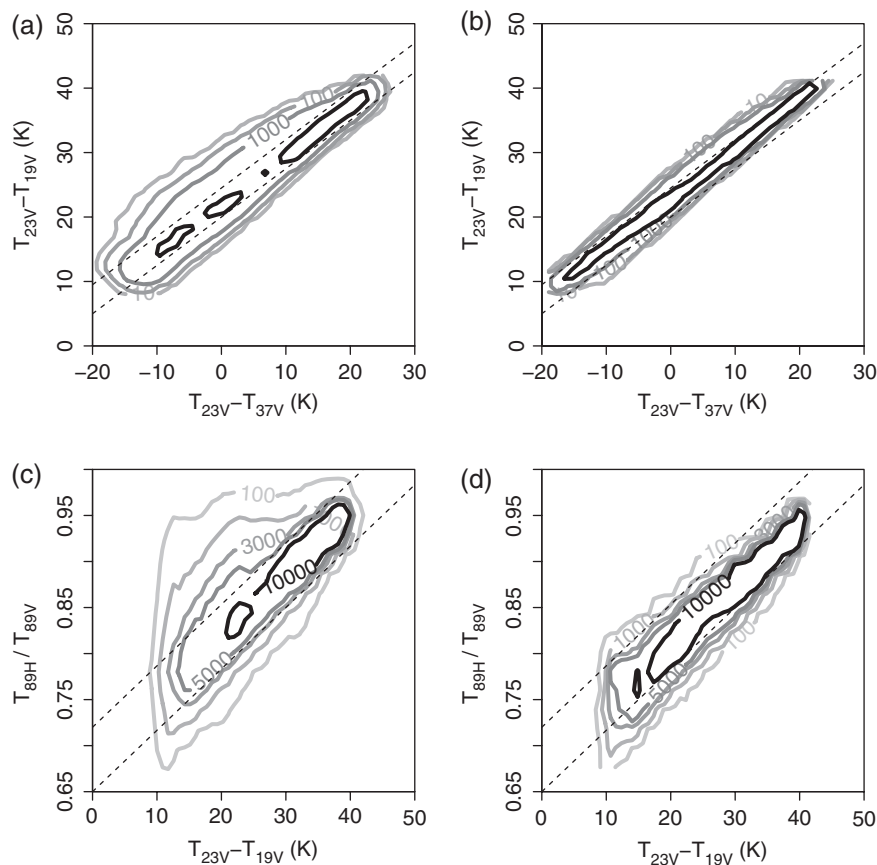


Figure 1. Data frequency distributions in cloud-screening parameter space for AMSR data on 1 August 2003. (a) $T_{23V} - T_{37V}$ and $T_{23V} - T_{19V}$ for observed radiance, (b) $T_{23V} - T_{37V}$ and $T_{23V} - T_{19V}$ for simulated clear-sky radiance, (c) $T_{23V} - T_{19V}$ and T_{89H}/T_{89V} for observed radiance, (d) $T_{23V} - T_{19V}$ and T_{89H}/T_{89V} for simulated clear-sky radiance. The contour lines indicate the data counts.

are described in the appendix. In airborne radiometer field experiments during the 1990s, the azimuthal variation was clearly observed (Etkin *et al.*, 1991; Dzura *et al.*, 1992; Yueh *et al.*, 1995, 1997, 1999). The signals vary as a function of the azimuth angle, wind speed and incidence angle. In theoretical studies on the ocean surface emissivity (Tsang, 1991; Yueh *et al.*, 1994; Yueh, 1997), their models were able to explain the azimuthal variation in horizontally and vertically polarized radiance, and in the third and fourth Stokes parameters. Moreover, the signal was found in analyses of space-borne radiometer measurements from the Special Sensor Microwave/Imager (SSM/I: Wentz, 1992; Meissner and Wentz, 2002). These experiments and analyses showed that radiances at 19 and 37 GHz have dependencies on wind direction relative to the sensor viewing angle. In other words, the directional features of ocean surfaces can be measured as the azimuthal

variation of the radiances. In geophysical parameter retrievals (e.g. sea-surface temperature, sea-surface wind speed and total column water vapour) from the satellite radiance data, the directional signal has been thought of as one of the error sources and been removed to obtain accurate geophysical parameters. Moreover, the signals are actively used as a geophysical model function (GMF) in wind vector retrievals from scatterometers (QuikSCAT, ASCAT) and WindSat measurements.

Wentz (1997) showed that inclusion of the azimuthal variation in a wind speed retrieval algorithm can significantly improve the accuracy of the wind speed product. Meissner and Wentz (2002) proposed an ocean emissivity model for the oceanic geophysical parameter retrievals, and recently their model was updated (Meissner and Wentz, 2012). Their latest model has an updated function to express the azimuthal variation in terms of

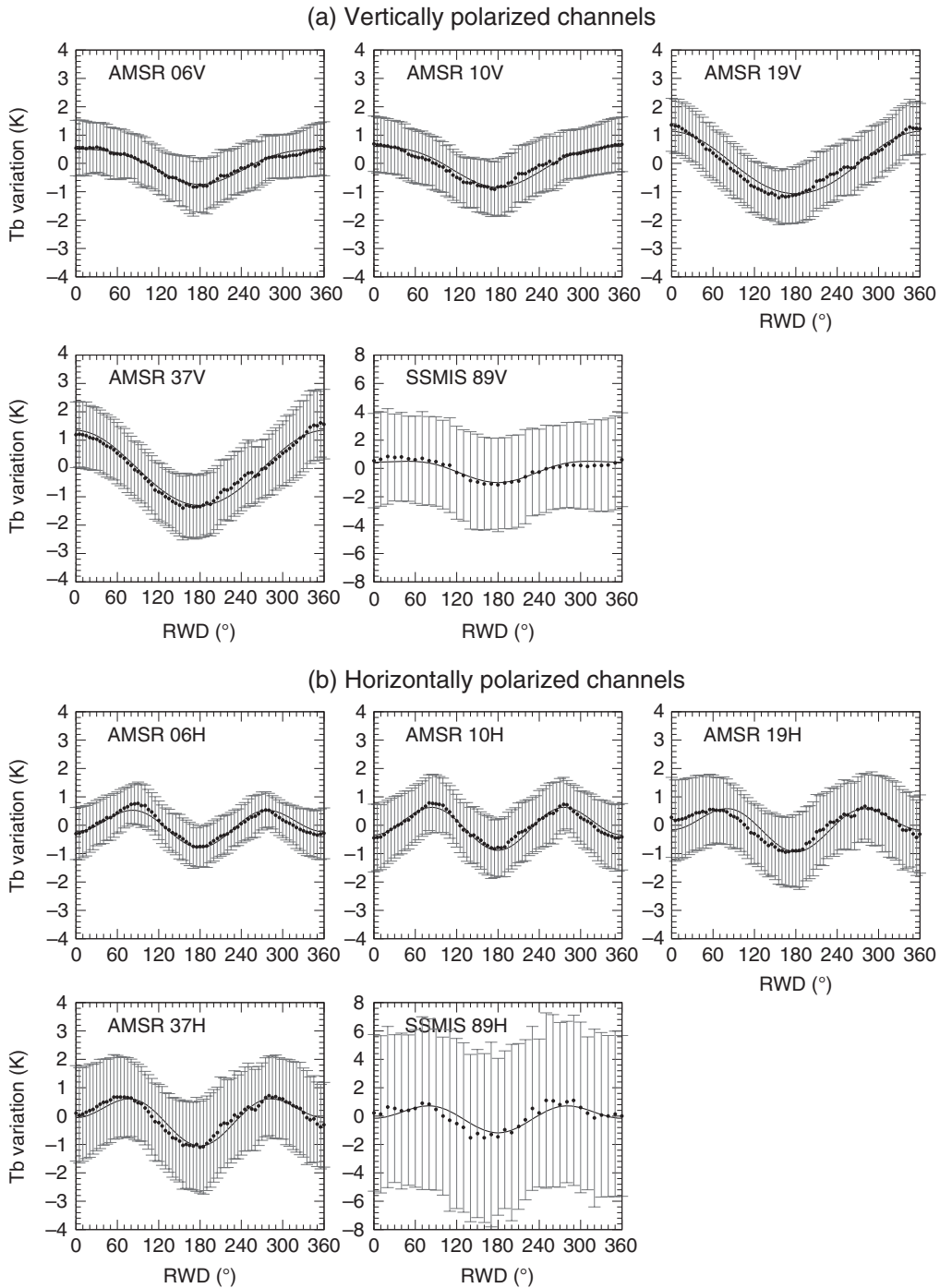


Figure 2. Oceanic microwave radiance variation in terms of RWD for surface wind speed 12 m s^{-1} . Panels (a) are vertically polarized channels and panels (b) are for horizontally polarized channels. AMSR radiance and SeaWinds wind vector were used for 6, 10, 19 and 37 GHz. F17 SSMIS radiance and surface wind vector from ECMWF IFS were used (see text section 2.2) for 89 GHz. The biases (black filled circles) and standard deviation (error bars) were plotted and fitted model functions were drawn with a black solid line.

a relative wind direction. The relative wind direction (RWD) is a wind direction relative to the satellite azimuth angle. Their model function was developed based on a collocated dataset of radiance measurements from WindSat and SSM/I, and wind observations from QuikSCAT.

In radiance data assimilation communities, a FAST microwave Emissivity Model (FASTEM) was developed (English and Hewison, 1998) for radiative transfer models RTTOV (Saunders *et al.*, 1999) and the Community Radiative Transfer Model (CRTM; Weng *et al.*, 2005). FASTEM is a semi-empirical model and has been widely used in many operational NWP centres, with the aim of computationally fast and accurate results. The initial version of FASTEM (FASTEM-1) was based on a geometric optics (GO) model simulation results. An updated version, FASTEM-2, by Deblonde and English (2001) was released in RTTOV-7 (Saunders *et al.*, 2002). An azimuthal variation model

function was introduced for the first time in FASTEM-3 (Liu and Weng, 2003), released as part of RTTOV-8 (Saunders *et al.*, 2006). In FASTEM-4 (Liu *et al.*, 2011), an updated permittivity calculation, new parametrizations of the roughness effect, foam parametrization and a new azimuthal model function were introduced. FASTEM-5 again modified the large-scale roughness and foam parametrization. FASTEM-4 and -5 are incorporated in RTTOV-10 (Saunders *et al.*, 2012) and RTTOV-11 (Saunders *et al.*, 2013). The impact of FASTEM-4 and FASTEM-5 for NWP was evaluated at the European Centre for Medium-range Weather Forecasts (ECMWF) and FASTEM-5 was selected for operational use (Bormann *et al.*, 2011, 2012).

However, the azimuthal model function in FASTEM-3, -4 and FASTEM-5 have not been used for microwave imagers in the operational NWP centres because the sensor azimuth angle information is not always available in real-time radiance data and

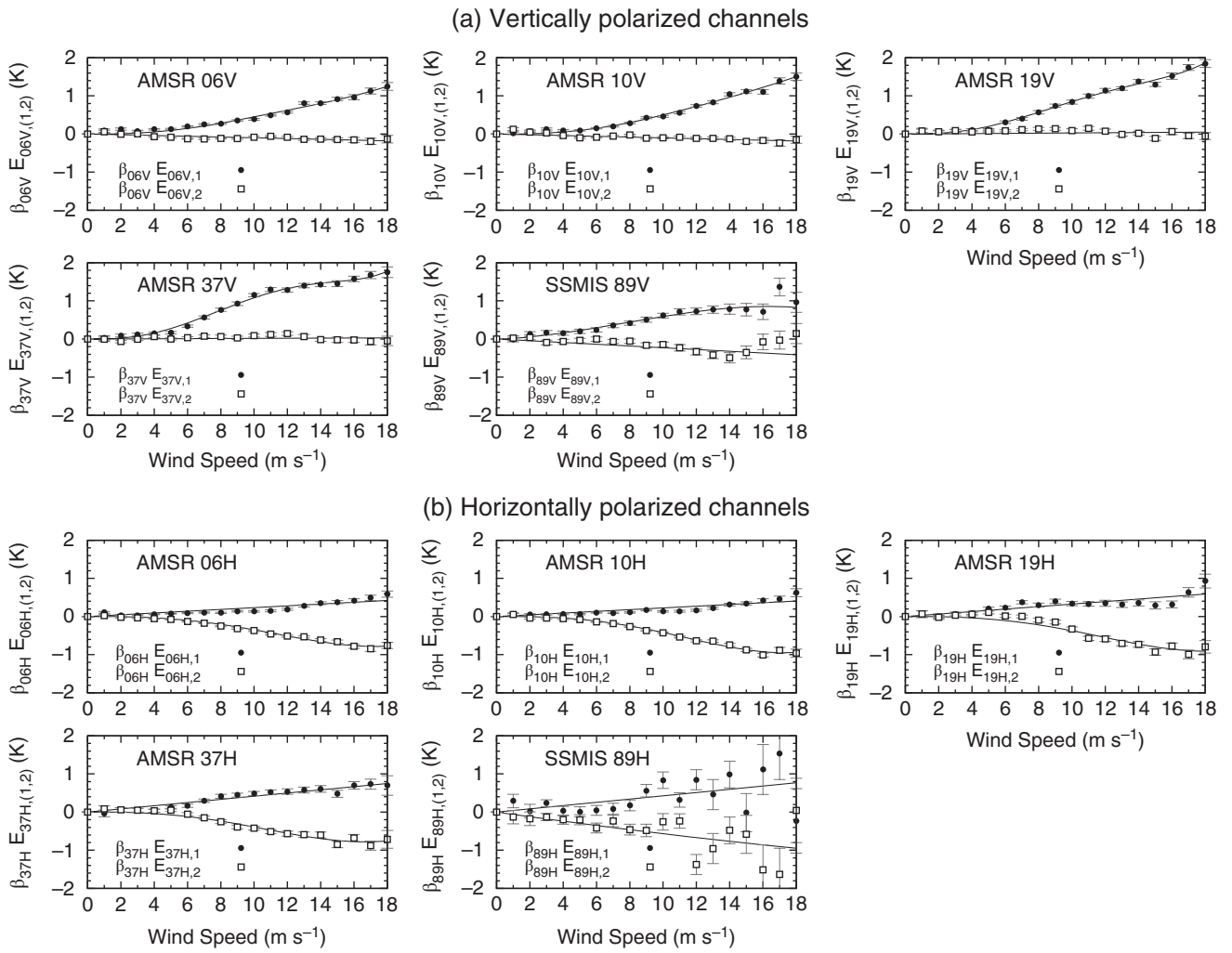


Figure 3. The amplitude of the harmonic cosine functions from the azimuthal variation. Black filled circles are the first harmonic term E_{i1} and white squares are the second harmonic term E_{i2} in Eq. (1). (a) Fitted functions for vertical channels in terms of wind speed with solid curves (Eqs (2) and (3)). (b) Same as (a) but for horizontal channels with solid curves (Eqs (4) and (5)). 06V, 06H, 10V, 10H, 19V, 19H, 37V, 37H are AMSR results and 89V and 89H are F17 SSMIS results.

Table 2. Estimated coefficients for the RWD model function.

Channel	a_{v1}	b_{v1}	c_{v1}	d_{v1}	α_v	a_{v2}	β_v
06V	4.394E-02	-1.636E+01	1.348E+00	-3.366E-02	5.828E-06	-3.513E-05	279.72
10V	4.397E-02	-1.639E+01	1.144E+00	-2.487E-02	5.445E-06	-3.604E-05	279.72
19V	5.009E-02	-1.638E+01	1.520E+00	-3.994E-02	1.330E-05	1.113E-05	246.15
37V	5.553E-02	-1.638E+01	1.602E+00	-4.246E-02	1.903E-05	7.524E-06	222.22
89V	-9.131E-05	1.251E+00	6.769E-01	-2.913E-02	1.092E+00	-1.806E-04	126.50
Channel	a_{h1}	a_{h2}	b_{h2}	c_{h2}	d_{h2}	α_h	β_h
06H	8.343E-05	-8.207E-03	-1.040E+01	4.536E-01	0.000E+00	2.589E-05	280.00
10H	8.082E-05	-8.204E-03	-1.040E+01	4.526E-01	0.000E+00	3.121E-05	280.00
19H	1.362E-04	-1.013E-03	-9.235E+00	3.844E-01	0.000E+00	2.891E-04	240.00
37H	1.910E-04	-2.224E-04	-9.232E+00	3.982E-01	0.000E+00	1.673E-03	218.18
89H	3.554E-04	5.226E-04	9.816E-01	-7.783E-03	0.000E+00	2.437E+01	120.00

because of insufficient modelling of the azimuthal variation in the emissivity model. The FASTEM-5 azimuthal model function is employed for microwave sounding instruments (e.g. Advanced Microwave Sounding Unit-A (AMSU-A), Microwave Humidity Sounder (MHS)) in the ECMWF system. However, because surface-sensitive window channels in the microwave sounding instruments (e.g. AMSU-A channels 1, 2, 3 and 4, MHS channels 1 and 2) are not actively assimilated (only used for quality-controlling the lower tropospheric channels), it is thought that the azimuthal variation of the surface emissivity in microwave sounding data has a minor effect on the data assimilation.

Furthermore, other biases in simulated radiance had been thought to be much larger than those from the surface wind direction signal. Therefore, the importance of the azimuthal

variation in the microwave imager measurements was thought to be negligible (Bormann *et al.*, 2011) and has been overlooked in the radiance assimilation communities. No investigations focussed on the effect of the azimuthal variation in the microwave radiance assimilation have been performed so far.

As shown in the literature on geophysical retrievals, the azimuthal variation reaches about 2 K in high wind-speed conditions. The phenomenon should be taken into account correctly in the calculation of microwave ocean emissivity for the radiance assimilation. Otherwise, the signals of the azimuthal variation may cause incorrect increments or excessive data rejection in the data assimilation, especially under strong wind conditions. Furthermore, the short-range forecast accuracy has increased significantly in recent years, so errors arising from the

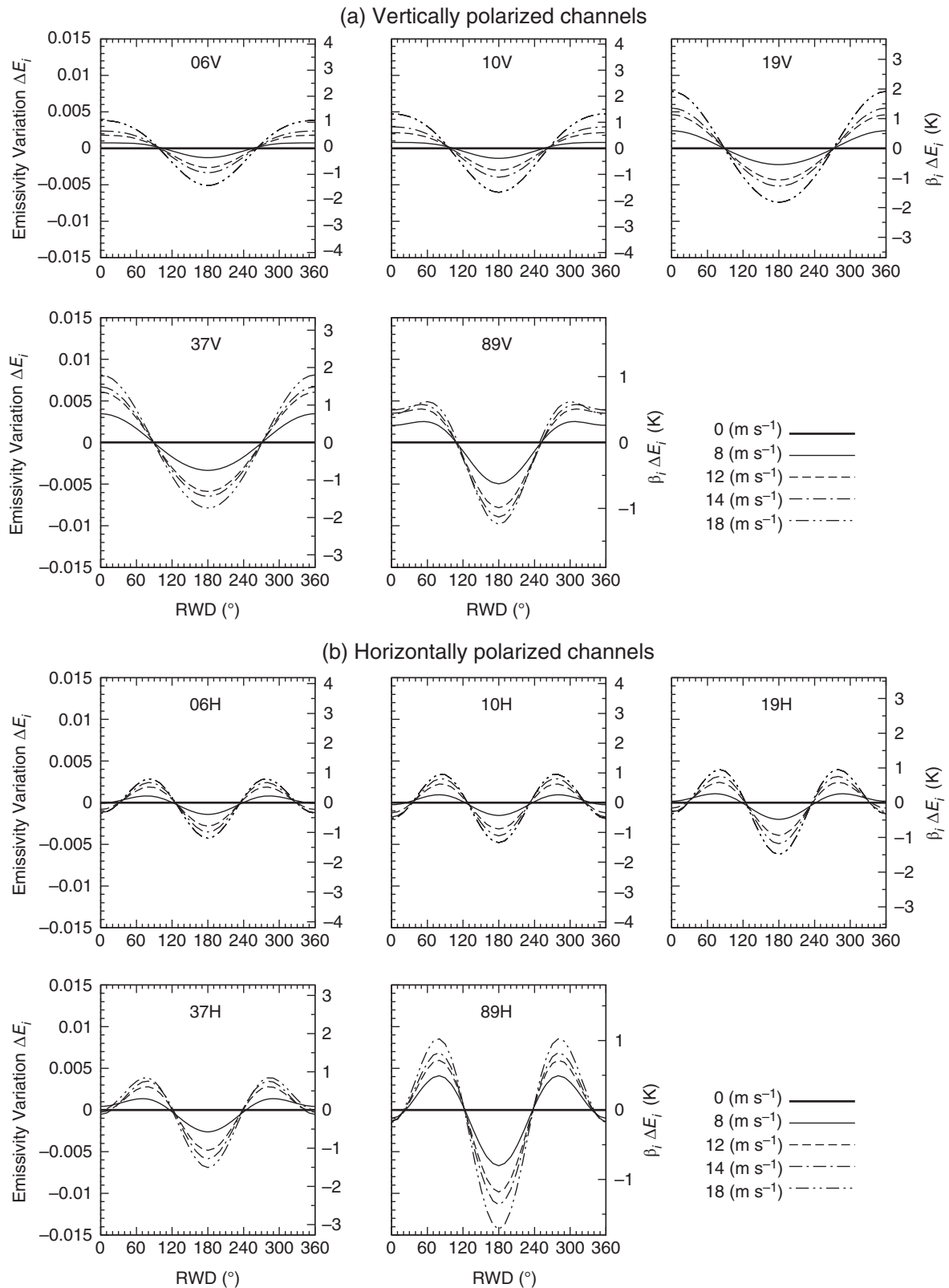


Figure 4. The azimuthal variation of the calculated emissivity with the developed RWD model function for 6–89 GHz. (a) Vertically polarized channels at 0, 8, 12, 14, 18 $m s^{-1}$ surface wind speed cases. (b) Same as (a) but for horizontally polarized channels. Right vertical axes are scaled in Kelvin by multiplying conversion coefficient β_i .

neglect of an azimuthal model function in the radiative transfer model are increasingly significant.

The goal of this study is to investigate the impact of the wind directional signal in the microwave radiance assimilation. To achieve this, the missing sensor azimuth angles in the real-time data are calculated based on satellite sensor locations and scan geometry for the Tropical Rainfall Measuring Mission (TRMM) Microwave Imager (TMI) and Special Sensor Microwave Imager/Sounder (SSMIS). We developed a new relative wind direction (RWD) model function to express the azimuthal

variation for the microwave radiance assimilation. The RWD model function was compared with present model functions in FASTEM-5 and FASTEM-3, and we performed a data assimilation experiment using the RWD model function to examine its scientific impacts.

In section 2, we describe the microwave ocean emissivity models, the derivation of the RWD model function and their comparison results. In section 3, the impact study and the experimental results are given. In section 4, we discuss our results and provide our conclusion.

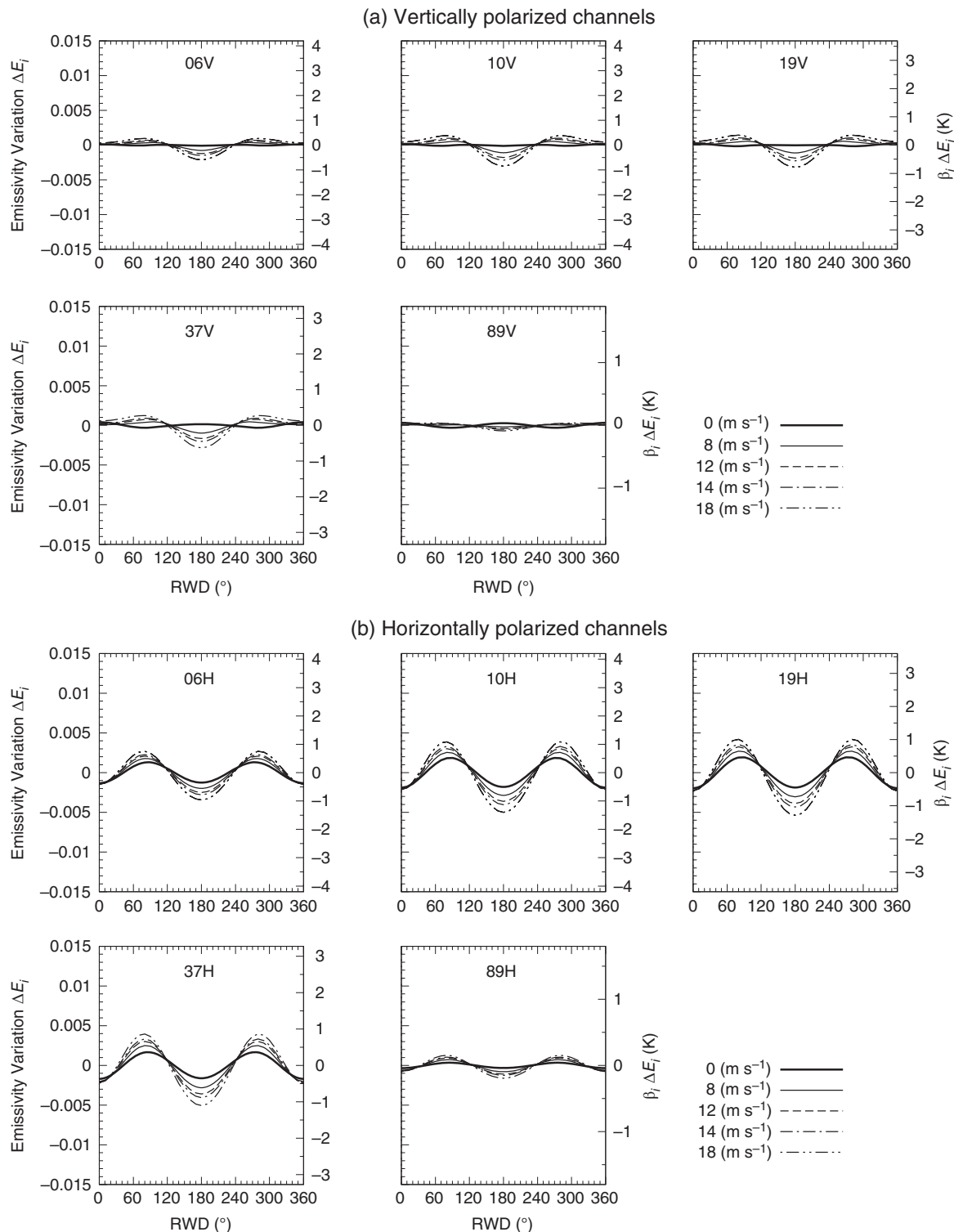


Figure 5. Same as Figure 4 but for FASTEM-5 azimuthal model function in RTTOV.

2. Modelling of microwave ocean surface emissivity

2.1. Design of model

A calm ocean surface is characterized by a polarized emission. The emissivity can be calculated assuming specular reflection using the Fresnel equation (e.g. Liou, 2002). The emissivity is a function of frequency, polarization, incidence angle, sea-surface temperature and salinity. When the surface is roughened by wind, the roughness of the surface increases the emissivity. In the modelling of microwave ocean emissivity, the roughness scales can be modelled with two scales. One is large-scale roughness, i.e. gravity waves or swell whose wavelengths are large compared with the microwave radiation wavelength. The other is small-scale roughness, i.e. capillary waves whose wavelengths

are small compared with the microwave radiation wavelength. The small-scale waves can be considered a modulation of the large-scale wave. Furthermore, the breaking waves produce foam and whitecap. They increase the emissivity because the foam and whitecap behave like a black body in the microwave frequency range.

These three contributions: (i) large-scale roughness, (ii) small-scale roughness, and (iii) foam and whitecap are parametrized and have been updated in the development of FASTEM.

2.1.1. Large-scale roughness effect

This phenomenon can be modelled as an ensemble of tilted facets, and each facet can be thought of as an independent specular surface. In FASTEM, this contribution is integrated

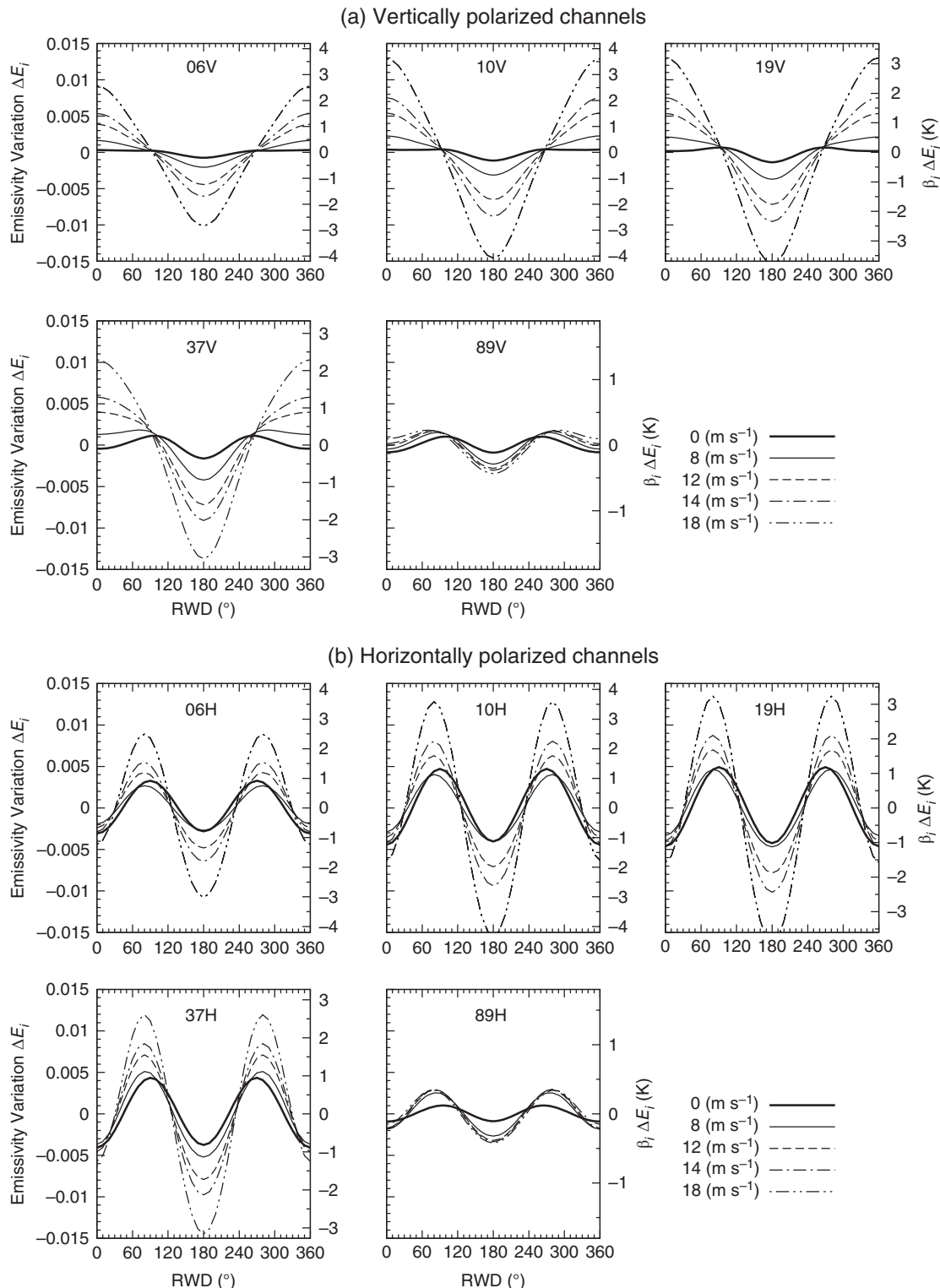


Figure 6. Same as Figure 4 but for FASTEM-5 azimuthal model function in CRTM.

and parametrized as a function of incident angle, wind speed and frequency to achieve the computational fast performance. FASTEM-1 parametrized the large-scale roughness effect based on a geometric optics (GO) model output. FASTEM-2 added a correction term to the reflectivity by using surface-to-space transmittance and updated the parametrization coefficients based on the GO model. The emissions from the large-scale wave are assumed to be isotropic in azimuthal direction.

2.1.2. Small-scale roughness effect

The roughness effect from the small-scale wave is a source of Bragg scattering and diffraction at the microwave frequency range. The small-scale roughness effect also increases the emission.

FASTEM-1 added an empirically derived correction factor (an exponential function of incidence angle) to the reflectivity. FASTEM-4 introduced an improvement to the roughness parametrization based on a two-scale emissivity model. Although the Bragg scattering by small-scale waves is the dominant effect in the directional signals (Yueh, 1997), there is no azimuthal dependence model function on the small-scale roughness effect in FASTEM because the surface spectrum was assumed to be isotropic.

2.1.3. Foam and whitecap

In FASTEM-1, -2 and -3, foam cover is modelled as a function of 10 m wind speed (Monahan and O'Muircheartaigh,

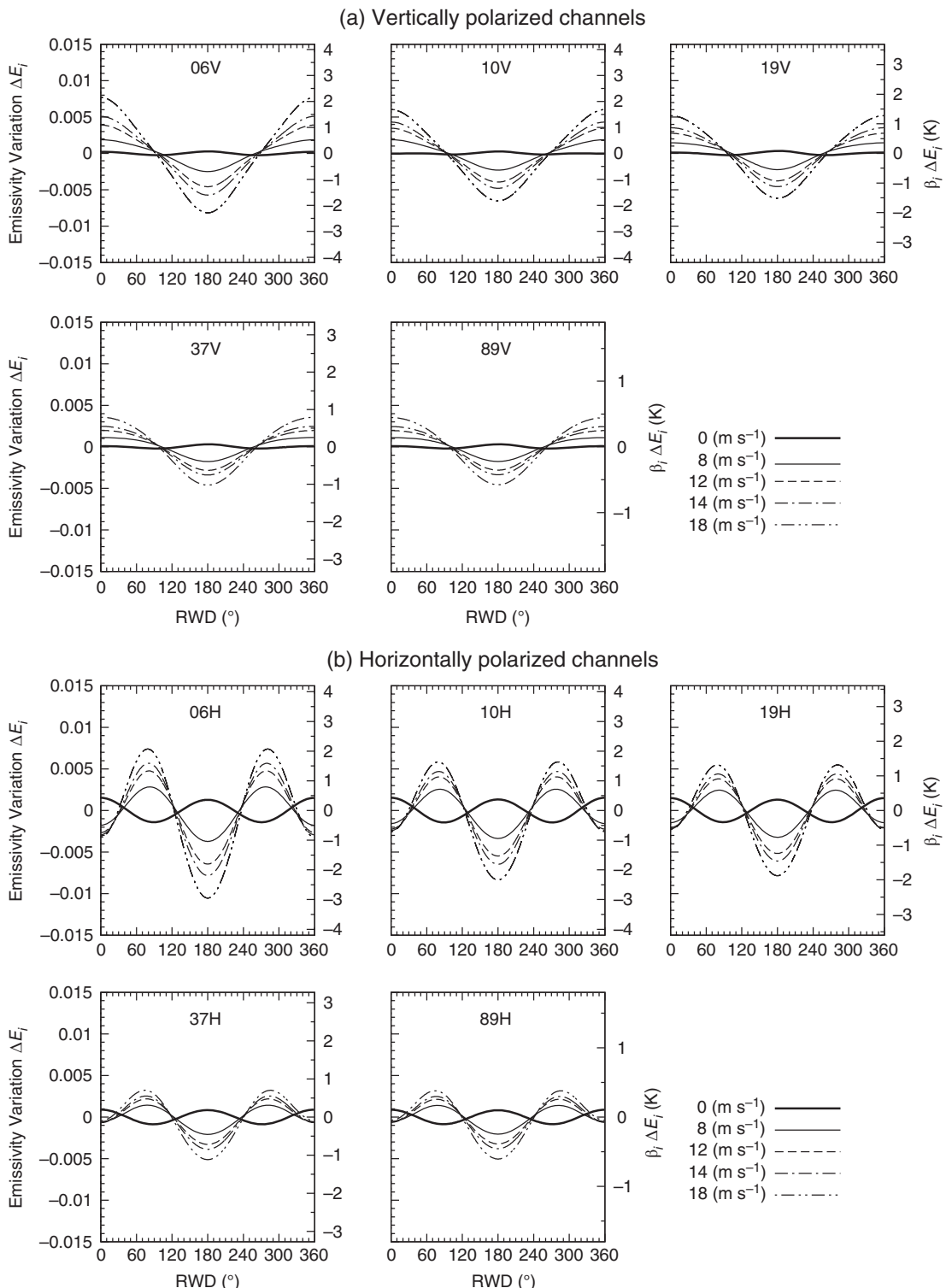


Figure 7. Same as Figure 4 but for FASTEM-3 azimuthal model function.

1986). Although FASTEM-4 introduced (Tang, 1974) foam cover parametrization, the model was changed from Tang (1974) to Monahan and O'Muircheartaigh (1986) in FASTEM-5. The foam functions are parametrized based on 10 m wind speed.

In addition to these three effects in FASTEM, a correction model to allow for the azimuthal variation of the emissivity was introduced for the first time in FASTEM-3 of RTTOV-8. The model was developed from measurements by the WindRad radiometer operated by the Jet Propulsion Laboratory and a model proposed by St. Germain *et al.* (2002) from aircraft measurements. FASTEM-3 uses a model function of azimuth line-of-sight less the wind direction. FASTEM-4 and FASTEM-5 updated the azimuthal function based on a theoretical two-scale model output, so are no longer based on real microwave

measurements from satellites. The FASTEM-4 and FASTEM-5 azimuth model functions use RWD as inputs to express the azimuthal variation instead of the azimuth line-of-sight less the wind direction. FASTEM-3 and FASTEM-5 use harmonic cosine functions to express the variation. The Meissner and Wentz (2012) model function uses similar harmonic cosine functions for the modelling.

Because observed azimuthal variation of the radiance showed harmonic cosine function's variation in terms of RWD space, our RWD model uses a second-order harmonic expansion as shown in Eq. (1). Coefficients in Eq. (1) have wind speed dependence. They are modelled with Eqs (2) and (3) for vertically polarized channels and Eqs (4) and (5) for horizontally polarized channels. The wind speed dependencies of the coefficients are different between the vertical and horizontal channels.

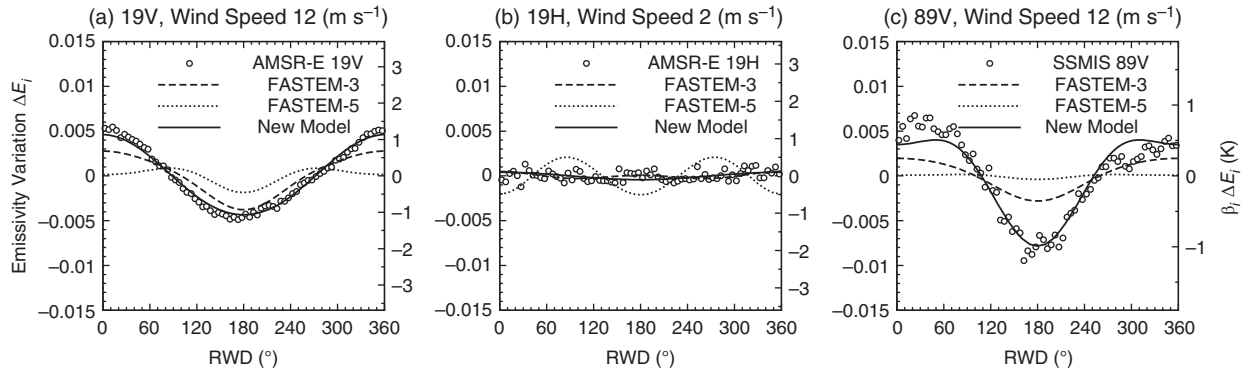


Figure 8. Comparisons of observed azimuth variation of the radiance and RWD models. (a) AMSR-E 19V at wind speed 12 m s^{-1} , (b) AMSR-E 19H at wind speed 2 m s^{-1} , (c) SSMIS 89V at wind speed 12 m s^{-1} .

For the vertically polarized channels, the first harmonic term is dominant and its amplitude increases with surface wind speed. This characteristic can be modelled with the third-order polynomial function in Eq. (2). For low wind-speed conditions ($< 7 \text{ m s}^{-1}$), the magnitude of the coefficients are small. However, they grow rapidly between 7 and 16 m s^{-1} . At high wind speeds ($> 16 \text{ m s}^{-1}$), the 19, 37 and 89 GHz vertically polarized channels wind-speed sensitivity saturates although no saturation is seen in horizontally polarized low-frequency channels. This characteristic can be modelled with an exponential term in Eq. (2). The variation of the second-term coefficients is relatively small compared to the first term. A linear function is therefore sufficient for the wind speed range from 0 to 18 m s^{-1} .

For the horizontally polarized channels, the second term in Eq. (1) is dominant. The variation of the second term in terms of wind speed is modelled with a third polynomial function and the exponential term as was the case for the first term for the vertical channels. The first term can be modelled with a linear function of surface wind speed, as was done for the second term of the vertically polarized channels. A similar approach is adopted in several studies, e.g. Wentz (1992), St. Germain *et al.* (2002), Meissner and Wentz (2002, 2012).

The RWD model is a function of RWD and surface wind speed and independent from other geophysical parameters (e.g. surface temperature, boundary-layer stability). This approximation is commonly used in other microwave emissivity models. It is possible that the azimuthal variation depends on other parameters, such as significant wave height, ocean current, or boundary-layer stability. But those are beyond the scope of our present study. The emissivity variations are modelled as the following equations:

$$\Delta E_i = E_{i1} \cos \phi_r + E_{i2} \cos 2\phi_r, \quad i = v \text{ or } h. \quad (1)$$

$$E_v1 = a_{v1} \{ \exp(-\alpha_v W^2) - 1 \} (b_{v1} W + c_{v1} W^2 + d_{v1} W^3), \quad (2)$$

$$E_{v2} = a_{v2} W, \quad (3)$$

$$E_{h1} = a_{h1} W, \quad (4)$$

$$E_{h2} = a_{h2} \{ \exp(-\alpha_h W^2) - 1 \} (b_{h2} W + c_{h2} W^2 + d_{h2} W^3), \quad (5)$$

where ΔE_i is the azimuthal variation of the microwave ocean emissivity for vertical or horizontal polarization channel. $\phi_r = \phi_w - \phi_s$ is the RWD defined from wind direction ϕ_w and satellite azimuth angle ϕ_s . W is the surface wind speed in m s^{-1} . The coefficients $a_{v1}, b_{v1}, c_{v1}, d_{v1}, \alpha_v, a_{v2}, a_{h1}, a_{h2}, b_{h2}, c_{h2}, d_{h2}$, and α_h were determined from fitting of the model to observed azimuthal variation for each frequency.

2.2. Data used and methodology

In order to determine the coefficients of the RWD model function, truth data of microwave radiance and surface wind vector are necessary. In the literature (Wentz, 1992; Meissner

and Wentz, 2002, 2012), collocated data between satellite microwave measurements and buoy wind data, or microwave measurements and scatterometer wind data were used. The amount of the collocated data between different platforms is very limited and it is difficult to collect a sufficient data sample covering varied meteorological condition (e.g. from low wind speed to high wind speed) with a short period. In this study, we use simultaneous measurements of radiance and wind vector by the Advanced Earth Observing Satellite-II (ADEOS-II). The Advanced Microwave Scanning Radiometer (AMSR) and National Aeronautics and Space Administration (NASA) scatterometer SeaWinds were aboard the satellite. The ADEOS-II data are available for seven months (April–October 2003). Temperature and specific humidity profiles and surface temperature from ECMWF reanalysis data (ERA Interim: Dee *et al.*, 2011) were used for simulation of AMSR radiance in radiative transfer calculations. Ebuchi (2006) reported on the accuracy of ADEOS-II SeaWinds wind data. No systematic biases in the wind speed and direction against buoys were confirmed. Root mean square (RMS) differences of the wind speed and direction were approximately 1 m s^{-1} and 20° in the buoy wind speeds higher than 3 m s^{-1} . Moreover, SeaWinds wind data had less correlation with the thermal condition of the sea surface and the sea state. SeaWinds wind data are used as the inputs of surface wind information in the radiative transfer calculations and the model function developed in our study.

The radiative transfer calculations were performed in clear sky conditions with RTTOV-10, but the azimuthal function in FASTEM-5 was turned off to visualize the azimuthal variation in the difference of the observed and simulated AMSR radiances. The AMSR channels cover the microwave frequency range from 6 to 89 GHz. The precise frequencies used in space-based microwave imagers vary from sensor to sensor. Table 1 summarizes the frequencies and channel numbers, for available microwave imagers in the data assimilation. Hereafter, we use notations defined in Table 1 to specify microwave imager channels.

To separate cloud signal and surface signal in the observed AMSR radiances over oceans, cloud-free scenes were selected. We used an empirical cloud-screening method. We define two indexes (S_{idx} and P_{idx}) in the following equations:

$$S_{\text{idx}} = (T_{23V} - T_{19V}) - C_s \cdot (T_{23V} - T_{37V}), \quad (6)$$

$$P_{\text{idx}} = (T_{89H}/T_{89V}) - C_p \cdot (T_{23V} - T_{19V}), \quad (7)$$

where $T_{19V}, T_{23V}, T_{37V}, T_{89V}$ and T_{89H} are observed AMSR radiances. We select AMSR data satisfying the following criteria:

$$S_{\min} < S_{\text{idx}} < S_{\max}, \quad (8)$$

$$P_{\min} < P_{\text{idx}} < P_{\max}, \quad (9)$$

where $C_s = 30.0/40.0$, $C_p = 0.2/30.0$, $S_{\min} = 20.0$, $S_{\max} = 24.5$, $P_{\min} = 0.65$, and $P_{\max} = 0.72$. These thresholds were

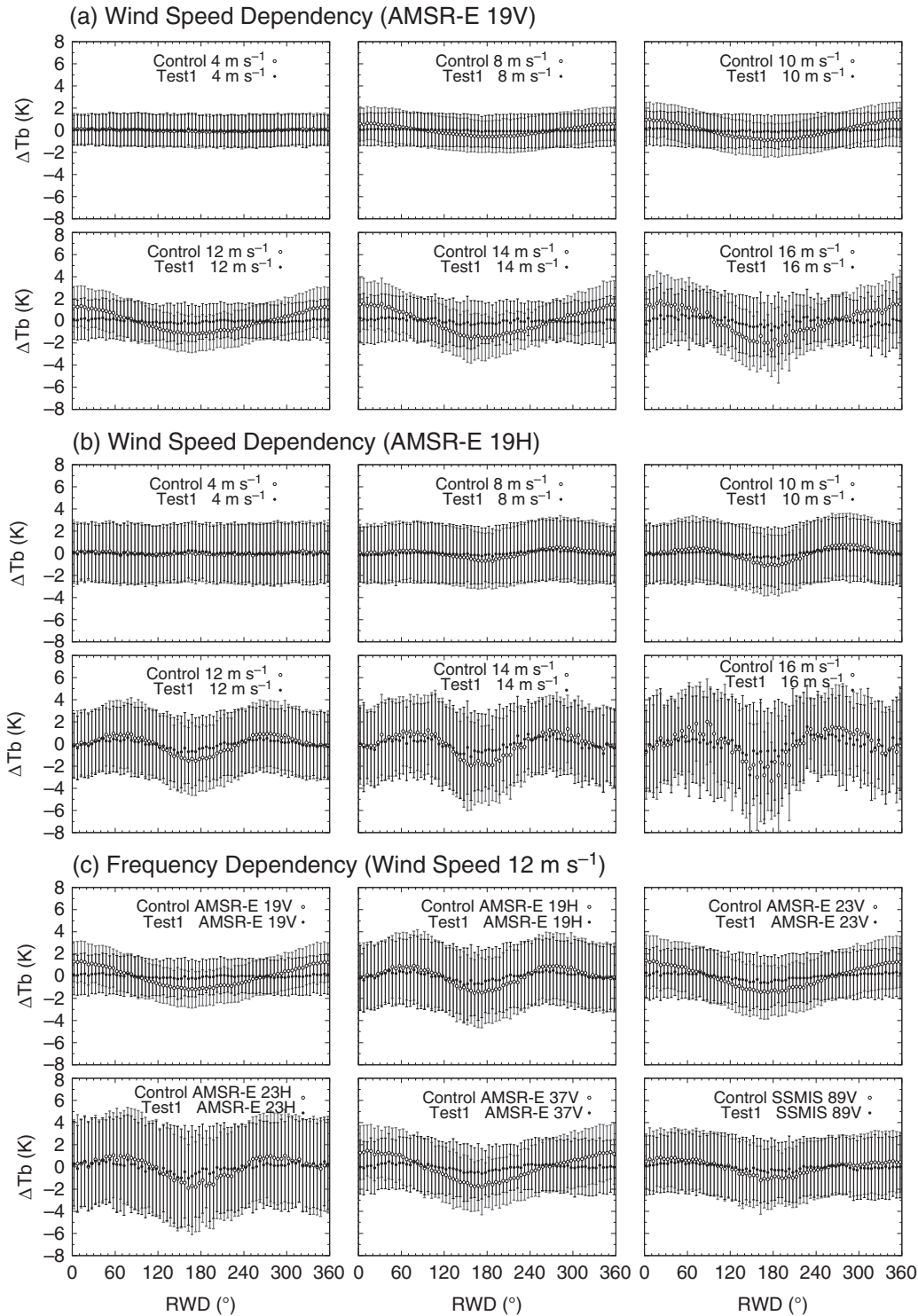


Figure 9. Comparisons of FG departure in terms of RWD between Test1 and the Control run for microwave imagers. The biases (Test 1: filled circles, Control: open circles) and the standard deviations (Test1: solid bars, Control: grey bars) are displayed. (a) AMSR-E 19V channel at 4, 8, 10, 12, 14, 16 m s⁻¹ surface wind speed, (b) same as (a) but for AMSR-E 19H channel, (c) AMSR-E for 19V, 19H, 23V, 23H, 37V and SSMIS for 89V. These are comparisons between RWD model function and no azimuth model function.

empirically determined. This empirical cloud detection is based on the cross-spectral variation of radiances, which is different between clear and cloudy conditions. Figure 1 shows examples of the relationship between indices for (a) observed AMSR radiance and (b) simulated clear sky radiance on 1 August 2003. Panel (a) indicates the relationship between $T_{23V} - T_{37V}$ and $T_{23V} - T_{19V}$ for observed radiance. Panel (b) indicates the same relationship but for simulated radiance under clear conditions, and shows the two amounts ($T_{23V} - T_{37V}$ and $T_{23V} - T_{19V}$) have a linear relationship in clear conditions. In other words, the two amounts are proportional in a situation with less cloud and rain (i.e. only water vapour is dominant). Two dashed lines in (a), (b) indicate the threshold (S_{\min} and S_{\max}). Furthermore, T_{37V} has

a larger cloud liquid sensitivity than T_{19V} . When the observed radiances are largely cloud affected, the data deviate from this relationship. Panels (c) and (d) show relationships of T_{89H}/T_{89V} and $T_{23V} - T_{19V}$ for observed radiance and simulated clear sky radiance, respectively. Most of the simulated data in the clear sky condition lie between the two dashed lines in the diagram. Observed radiances at 89 GHz are much more sensitive than those of 19 or 23 GHz. Therefore, observations falling outside the area between the dashed lines can be thought of as cloud- or rain-affected data. They are removed from the dataset for the coefficient fitting. The parameters C_s , C_p mean gradients and S_{idx} , P_{idx} mean intercepts in the diagrams. This cloud screening is independent of satellite azimuth angle, surface wind speed and

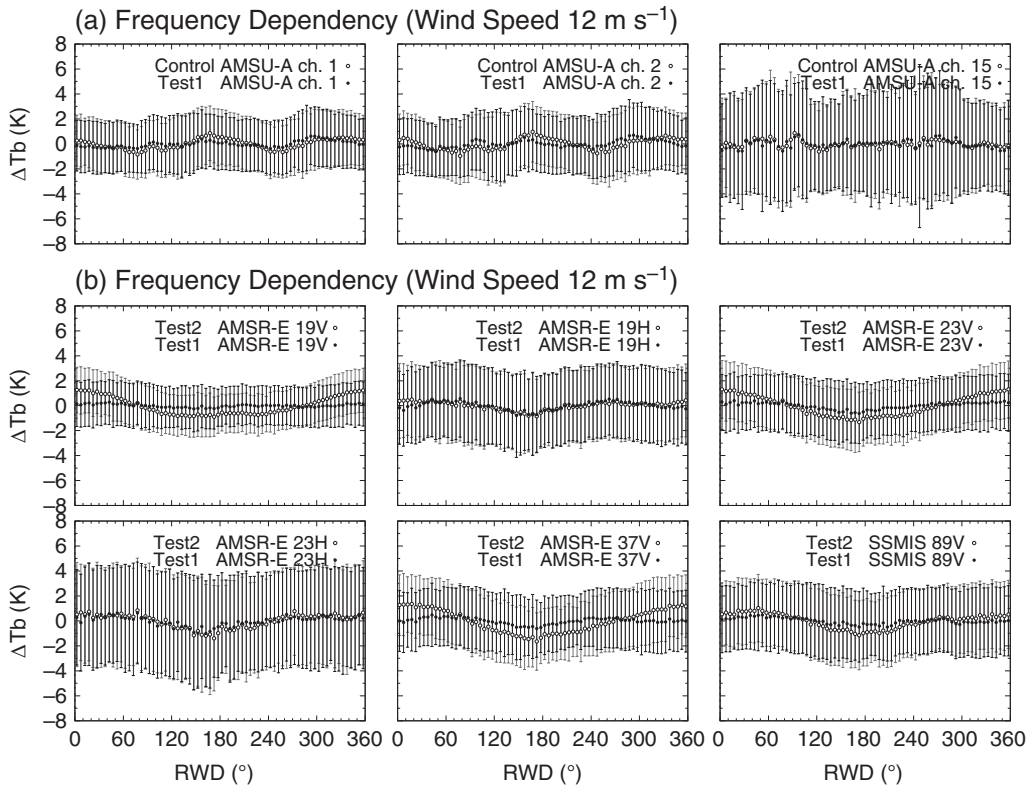


Figure 10. (a) Comparisons of FG departure in terms of RWD between Test1 and the Control run for surface-sensitive microwave sounder channels. The biases (Test1: filled circles, Control: open circles) and the standard deviations (Test1: solid bars, Control: grey bars) are displayed for Metop-A AMSU-A channels 1, 2 and 15 at surface wind speed 12 m s^{-1} . These are comparisons between our RWD model function and FASTEM-5 azimuth model function. (b) Comparisons of microwave imager FG departure between our RWD model function (Test1: filled circles) and FASTEM-5 (Test2: open circles) for AMSR-E 19V, 19H, 23V, 23H, 37V and SSMIS 89V at 12 m s^{-1} surface wind speed.

direction. Moreover, we require that the difference of the observed and simulated radiance should be within 5.0 K to remove cloud-contaminated data. Sun-glint-affected data in AMSR data were removed in advance.

In conversion of the radiance's variation to the emissivity variation, atmospheric transmittance should be taken into account. General microwave radiative transfer can be described by the following equation (equation (6.8) in Janssen (1993)).

$$T_b(v, \theta) = T_u(v, \theta) + \{\varepsilon_s T_s + (1 - \varepsilon_s) T_d(v, \theta)\} e^{-\tau(0) \sec \theta} \quad (10)$$

The left-hand side is observed radiance $T_b(v, \theta)$ with frequency v and incidence angle θ . On the right-hand side, T_u is upwelling radiation, T_d is downwelling radiation, ε_s is surface emissivity, T_s is surface temperature, and $e^{-\tau(0) \sec \theta}$ is atmospheric transmittance. Higher-frequency channels have smaller transmittance than those of low-frequency channels in atmospheric profiles under clear sky conditions. Therefore, radiance variations are converted differently depending on mean atmospheric transmittances in the channel's microwave frequency. Conversion coefficients β_i from the radiance to the emissivity are necessary to obtain the final coefficients used in our model:

$$\Delta T_b = \beta_i \Delta E_i, \quad (11)$$

$$\beta_i = T_s e^{-\tau(0) \sec \theta}. \quad (12)$$

The coefficients β_i can be thought of as a global mean of surface temperature multiplied by mean atmospheric transmittance for each channel. The β_i were determined by using atmospheric profiles to produce the same amplitude of the azimuth variation between observed and simulated radiances. This is possible because we assume the RWD model function is purely dependent on surface wind and there is no dependency on sea-surface temperature or atmospheric properties. Because high-frequency channels, e.g. 89 GHz, are sensitive to clouds in the atmosphere,

the 7-month ADEOS-II period was not sufficient to estimate the azimuthal variation in the all wind-speed categories. Therefore, we used all-sky F17 SSMIS data instead of AMSR for the 89 GHz channels. The SSMIS has 91 GHz vertically and horizontally polarized channels. The simulated all-sky SSMIS data were obtained from the ECMWF Integrated Forecasting System (IFS), using cycle 38r2 and run at a horizontal resolution T511 (with a 32 km grid) L137 (with 137 vertical levels) compared to operational resolution in June 2013 of T1279 (with a 16 km grid) L137. No azimuthal model function in the radiative transfer model (RTTOV-10) was used. We determined all the coefficients for 6, 10, 19, 37 and 89 GHz in vertical and horizontal polarization. A linear interpolation in frequency is used to obtain intermediate frequencies (e.g. 23 GHz) needed for other microwave instruments. Thus, our RWD model function is applicable to the Advanced Microwave Scanning Radiometer for Earth Observing System (AMSR-E: Kawanishi *et al.*, 2003), SSMIS and TMI that are actively used in data assimilation.

After subtraction of the mean bias in the difference of observed and simulated AMSR radiance for all wind-speed categories (1 m s^{-1} intervals, from 0 to 18 m s^{-1}), the remaining biases are attributed to the wind directional signal in terms of RWD. Figure 2 shows the variations in terms of RWD for a surface wind speed of 12 m s^{-1} . In each panel, the vertical axis indicates the difference between observed and simulated radiance after the bias subtraction. The horizontal axis is RWD defined from SeaWinds wind direction and AMSR azimuth angle. Figure 2(a) panels are vertically polarized channels and Figure 2(b) panels are horizontally polarized channels. Our RWD model function was fitted to the bias between the observed and simulated radiance. The fitting was performed for a wind speed range from 0 to 18 m s^{-1} in 1 m s^{-1} intervals to obtain the wind speed dependency for the coefficients.

A small phase shift between measured RWD signal and fitted model function exists. The phase shift was pronounced in high wind-speed conditions ($> 12 \text{ m s}^{-1}$). At present, we do not know

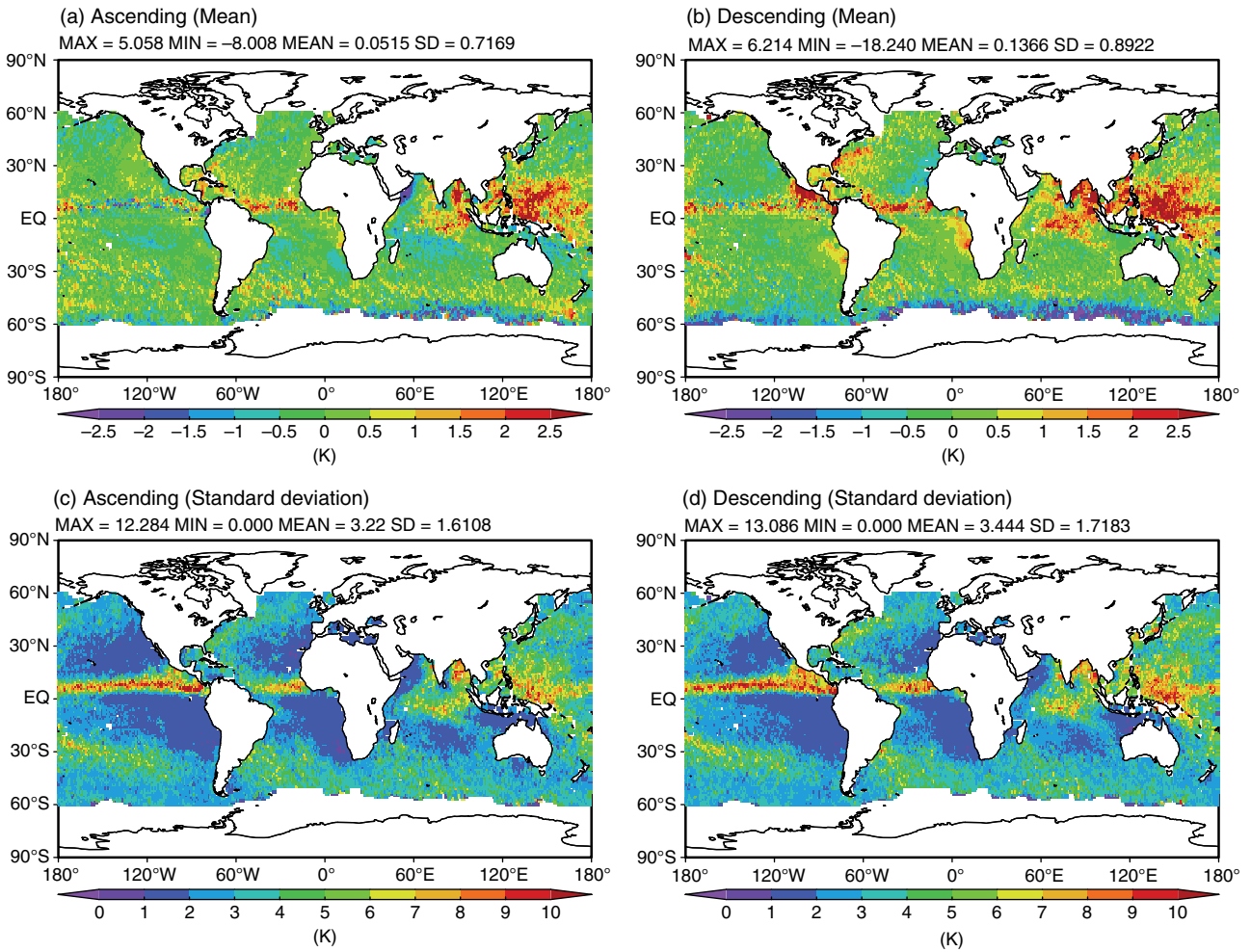


Figure 11. Mean and standard deviation of FG departure of F17 SSMIS 19V channel from the Control run in the experiment period. The ascending data are (a) mean, (c) standard deviation. The descending data are (b) mean, (d) standard deviation.

the reasons for these discrepancies. However, the small phase shifts did not affect the estimation of the amplitude of the variation in the wind speed range.

Figure 3 shows the coefficients obtained from the fitting for the RWD model function. The coefficients of the first harmonic term are shown in black solid circles. For the second harmonic term they are shown in white squares. Fitted functions are drawn with solid lines. The first harmonic term is dominant for vertical polarization channels and the second harmonic term is dominant for horizontal polarization channels. These results are consistent with other investigations (Meissner and Wentz, 2002, 2012). Large variations of the directional signal in radiance are found. Moreover, wind directional signals for the high-frequency channels (89V and 89H) are found, while the FASTEM-5 azimuth model function in RTTOV has very weak sensitivity for these channels (Figure 5). Table 2 shows the estimated coefficients for the dual polarization channels of AMSR from 6 to 89 GHz. Tangent linear and adjoint models of the RWD model function were developed for use in variational data assimilation.

2.3. Comparison with other RWD model functions

We compared our RWD model function performance with other azimuthal model functions. Currently, FASTEM-5 and FASTEM-3 have different azimuthal model functions for the data assimilation. Figure 4 indicates calculated emissivity variation from our RWD model function for 6, 10, 19, 37 and 89 GHz at wind speeds of 0, 8, 12, 14 and 18 m s⁻¹. Figures 5, 6 and 7 are as Figure 4 but for the FASTEM-5 (in RTTOV and in CRTM) and FASTEM-3 azimuthal model function, respectively. Right vertical axes are scaled in Kelvin in the Figures. The mean biases in each

wind speed category were subtracted to show only the azimuthal variation. Comparing Figures 4 and 5, we found that our RWD model function has a larger amplitude in terms of wind speed than FASTEM-5 in RTTOV. Our RWD model function was derived from real microwave radiance measurements, while FASTEM-5 was based on a theoretical two-scale model simulation results. The amplitudes of FASTEM-3 (Figure 7) are similar to our RWD model. However, FASTEM-5 (Figure 5 and 6) and also FASTEM-3 have sensitivity in the 0 m s⁻¹ wind speed range (less than 0.5 m s⁻¹). This is unphysical behaviour. We designed our RWD model function to have no sensitivity on the azimuthal variation at 0 m s⁻¹ wind speed, because there is less wind direction signal in passive microwave measurements in such low wind-speed situations. The performance of azimuth variations of FASTEM-5 in RTTOV (Figure 5) and that in CRTM (Figure 6) show different wind-speed dependency. We have to compare these azimuth emissivity models to real observations. Figure 8 shows comparisons between observed radiance variation from AMSR-E and SSMIS and the model simulations. Figure 8(a) shows the AMSR-E 19 GHz vertically polarized channel. Our RWD model and FASTEM-3 are closer to the observations than FASTEM-5. Figure 8(b) indicates a case of low wind speed (2 m s⁻¹) for the 19 GHz horizontally polarized channel (AMSR-E 19H). FASTEM-5 shows a large sensitivity to RWD. Figure 8(c) indicates a case of high-frequency channel (89V for SSMIS). Our RWD model performances are close to the observed azimuth variation of SSMIS.

Measurements on the incidence angle dependency of the azimuthal variation are very limited, so we imported them from other studies (equation (26) in Meissner and Wentz (2012)) to add incidence angle dependency in our RWD model. This function is necessary to apply our RWD model function to cross-track microwave radiometers.

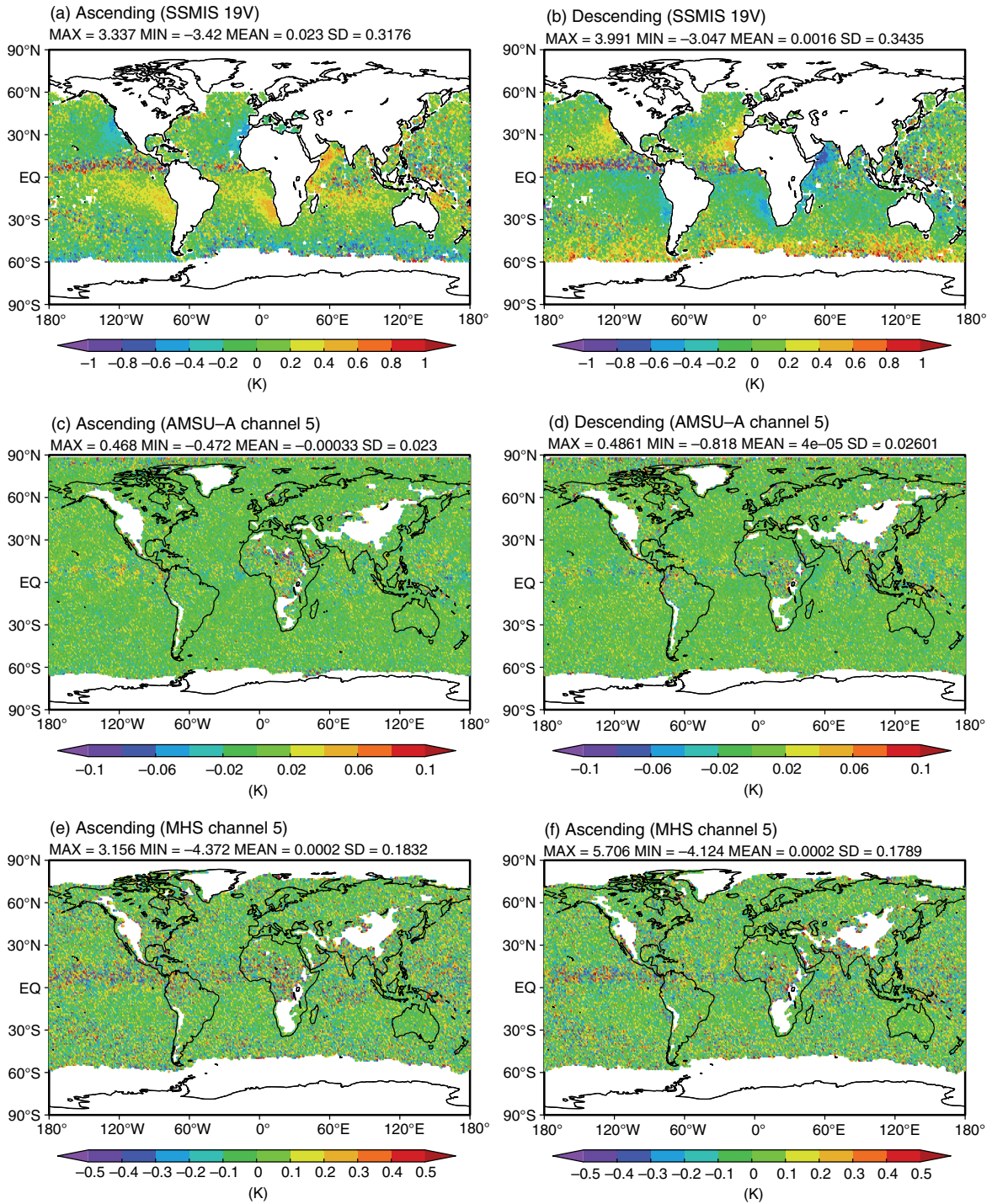


Figure 12. Mean difference of FG departure of assimilated data between Test1 and Control in the experiment period. (a) F17 SSMIS 19V ascending data, (b) descending data, (c) Metop-A AMSU-A channel 5 ascending data, (d) descending data, and (e) Metop-A MHS channel 5 ascending data, (f) descending data. The comparison is between our RWD model function and no azimuthal model function.

Over wind speed 18 m s^{-1} , ADEOS-II could not provide sufficient data for the fitting. For the high wind-speed cases ($>18 \text{ m s}^{-1}$), our RWD model assumes that the azimuthal variation has the same amplitude as for a wind speed of 18 m s^{-1} . No extrapolation with wind speed is used. Moreover, our model does not have the capability to calculate azimuthal variation on the third and fourth Stokes parameters.

3. Impact study

3.1. Experimental configuration

To examine the effect of the RWD model function in the data assimilation, we performed data assimilation experiments in the ECMWF Integrated Forecast System (IFS). In ECMWF IFS,

microwave imager radiance data are assimilated in an all-sky approach over ocean (Bauer *et al.*, 2010; Geer *et al.*, 2010; Geer and Bauer, 2011). The ECMWF IFS system (cycle 38r2: Bauer *et al.*, 2013) uses RTTOV-10 (Saunders *et al.*, 2012) as radiance observation operator in the data assimilation (Bormann *et al.*, 2011). We modified the FASTEM-5 azimuthal model function with our RWD model function for one of the experiments (Test1). The Control run does not use the azimuthal function in FASTEM-5 for the microwave imagers. As for microwave sounders (e.g. AMSU-A, MHS), the azimuthal model function in FASTEM-5 is used in the Control run. These settings of the Control run are consistent with the operational ECMWF IFS configuration. Our RWD model function is used for both microwave imager and sounder instruments in Test1. Because the surface-sensitive channels (e.g. AMSU-A, channels 1, 2, 3 and 4, MHS channels 1 and 2) are not actively assimilated in the ECMWF system, the

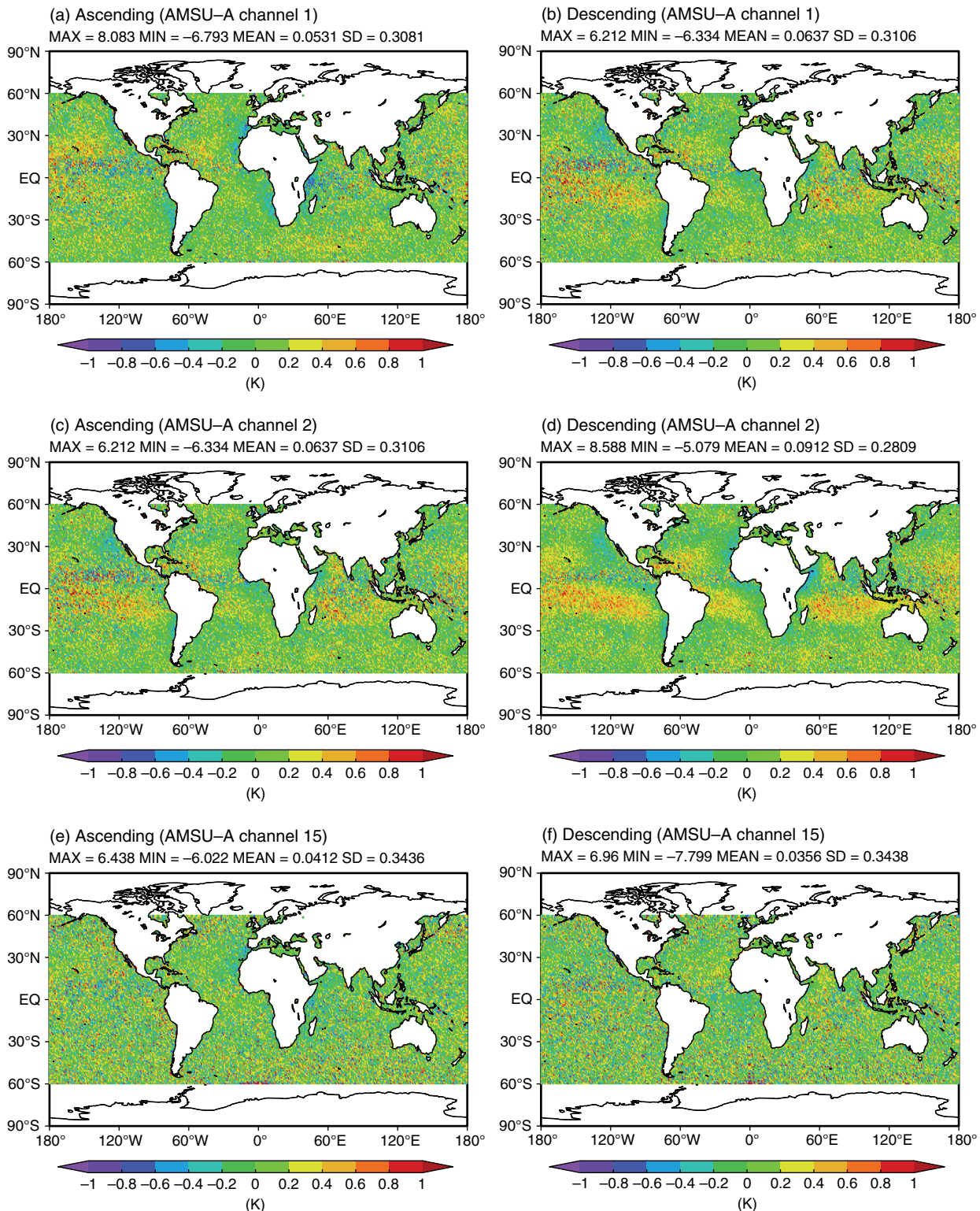


Figure 13. Mean difference of FG departure of surface-sensitive channels of Metop-A AMSU-A between Test1 and Control in the experiment period. (a) Channel 1 (23.8 GHz) ascending data, (b) Channel 1 descending data, (c) Channel 2 (31.4 GHz) ascending data, (d) Channel 2 descending data, and (e) Channel 15 (89.0 GHz) ascending data, (f) Channel 15 descending data. The comparison is between our RWD model function and FASTEM-5 azimuth model function.

change of the emissivity model for the microwave sounders should be minor, and major impact would be seen for the microwave imagers. As a comparison experiment, FASTEM-5 azimuth model function is used for microwave imagers and sounders in Test2.

Test1 uses our RWD model function for all microwave sensors, and Test2 uses FASTEM-5 azimuth model function for all microwave sensors. The Control uses no RWD model for microwave imagers and FASTEM-5 azimuth model function for microwave sounders.

The input RWD for the models is the difference between first-guess wind direction and the satellite azimuth angle at the observation locations. SSMIS and TMI do not have azimuth angles

available in the real-time dataset, so the angles were numerically calculated in house using the Kumabe and Egawa (2011) method from the satellite sensor position and scan geometry.

Observations used in the experiments are identical between the Test runs and the Control run. Quality control, pre-screening and the forecast model are also identical among the three runs. The only difference is the use of the RWD model function in the radiative transfer calculation. The experiments were executed at T511 L137 resolution with cycle 38r2 configuration. This was the operational cycle at ECMWF in June 2013, but in our experiments it was run at approximately half the operational resolution. The experiment period was from 20 June to 3 October 2011. The

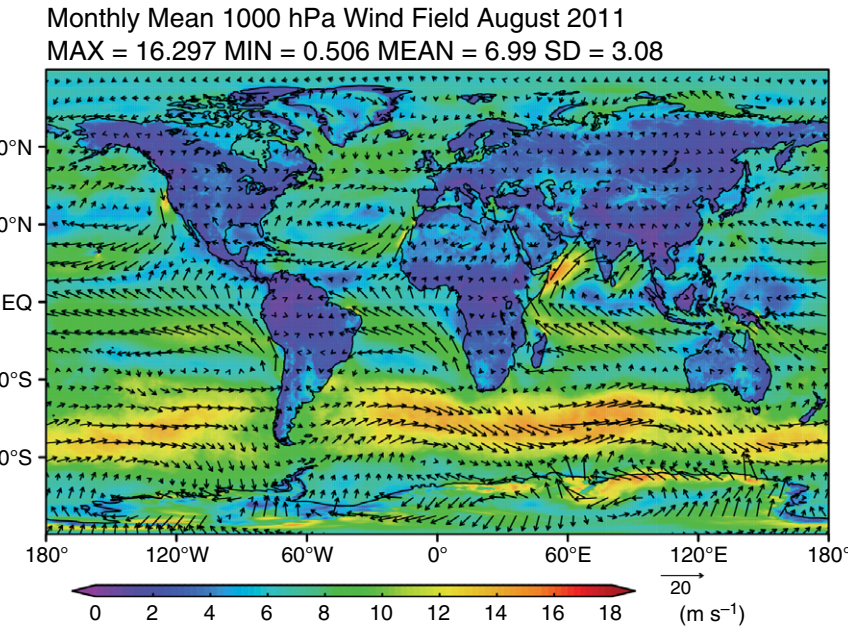


Figure 14. Monthly mean wind field at 1000 hPa for August 2011 in Test1.

forecasts from 0000 UTC initial times were produced every day during the period. Because three microwave imagers (AMSR-E, TMI and F17 SSMIS) were available in the experiment period, the large amount of radiance data would provide a strong test for the use of the RWD model function. The microwave imager channels 19V, 19H, 23V, 23H (for AMSR-E only), 37V and 89V were actively assimilated in the experiments. AMSR-E 89V and 89H channels were not available due to instrument issues during the period. In the ECMWF all-sky radiance assimilation scheme, horizontally polarized channels at 37 GHz and 89 GHz from microwave imagers are not assimilated.

3.2. FG departure comparison

The first guess (FG) is a short-range forecast (~ 12 h) valid at the time and location of the observations. FG departure is examined to investigate the impact of the RWD model function in the radiative transfer calculations. Figure 9(a) panels show bias (black dots for Test1 and open circle for Control) and standard deviation (solid bars for Test1 and grey bars for Control) for AMSR-E 19V FG departure at wind speed ($4, 8, 10, 12, 14$ and 16 m s^{-1}) categories. We used FG departure after variational bias corrections (VarBC; Dee, 2004) for these comparisons. In low wind-speed conditions (e.g. 4 m s^{-1}), the differences between Test1 and Control were small because the azimuthal variation itself was small. In high wind-speed conditions ($> 10 \text{ m s}^{-1}$), clear azimuthal variations in terms of RWD were found in the Control. This means the NWP FG wind field has sufficiently high accuracy in speed and direction to represent the azimuthal variation. The azimuthal variations in the biases were reduced in Test1. Figure 9(b) panels show the same results but for 19H. In high wind conditions (e.g. 16 m s^{-1}), the biases from the azimuthal variation reached about 2 K in the Control in both polarizations. However, in Test1, the RWD model function was able to represent the variation for both polarizations from the low to high wind-speed conditions and reduced the biases. Although the results in high wind conditions (Figure 9(b); $14, 16 \text{ m s}^{-1}$) show small remaining biases, generally most of the biases were reduced in Test1. Figure 9(c) panels indicate comparisons among different frequency (19V, 19H, 23V, 23H, 37V and 89V) at 12 m s^{-1} wind speed conditions. These microwave imager channels are actively assimilated in the ECMWF IFS. At 89V, the results for SSMIS were plotted instead of AMSR-E. For the frequency range from 19 to 91 GHz, the RWD model function reduced the biases and worked properly for AMSR-E, SSMIS and TMI. The results shown in Figure 9

are comparisons between using our RWD model function and using no azimuth model function (i.e. Test1 and Control) for microwave imagers. Figure 10(a) compares results for AMSU-A surface-sensitive channels using our RWD model function (Test1) and the FASTEM-5 azimuth model function (Control). In the Control run, the FASTEM-5 azimuth model function is used for microwave sounding sensors. Because AMSU-A is a cross-track scanning sensor, the incidence angle varies depending on the scan position, and the sensitivity to the surface wind also varies. These channels are not assimilated but their simulated radiance could be affected by the change of RWD model. No clear improvement was found for these channels but the new RWD model function appears to provide similar performance to FASTEM-5 here. Figure 10(b) shows comparisons between using our RWD model and the FASTEM-5 azimuth model function for microwave imagers (Test1 and Test2). Larger bias reductions using our RWD model function were confirmed.

Figure 11(a,b) show geographical distributions of mean FG departure of assimilated F17 SSMIS 19V in the Control. Moreover, (c) and (d) show standard deviation of the FG departure. Figure 11(a,c) are ascending data and (b) and (d) are descending data. In the Intertropical Convergence Zone (ITCZ) and South Pacific Convergence Zone (SPCZ), large positive biases (2–5 K) in FG departure were found for both ascending and descending orbit data (Figure 11(a,b)). Moreover, in the ITCZ and SPCZ, the standard deviations were larger than in other areas. The reason for the positive biases and the large standard deviation relates both to the accuracy of the radiative transfer model and the forecast model under cloud and precipitation conditions. They are similar in ascending and descending orbits. Because larger observation errors are assigned for these data in the ECMWF all-sky radiance assimilation system (Geer and Bauer, 2011), these biases are not as important as they look. However, the FG departure bias in the Arabian Sea was orbit dependent. The sign of the bias was opposite between the ascending orbit (negative bias approximately 1.5 K) and descending orbit (positive bias approximately 1.0 K) while the standard deviations in the area were relatively small (less than 2 K) compared with other areas. The orbit-dependent biases are large and might have a negative impact on forecast quality in the Control run.

Figure 12 shows the difference of mean FG departure between the Test1 and Control runs for F17 SSMIS 19V (a) ascending and (b) descending data. The impacts of the RWD model function varied between regions and orbital direction in the SSMIS FG departures. Generally, the orbit-dependent biases of

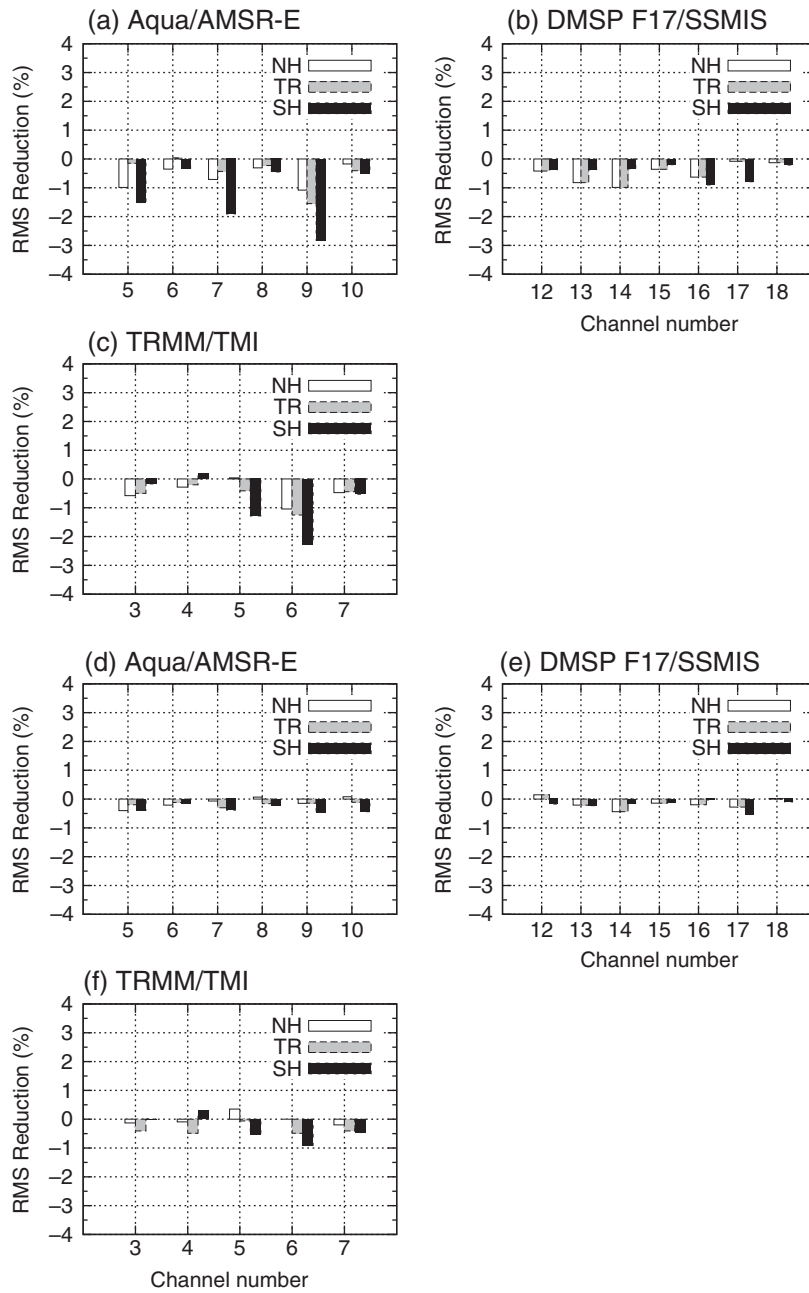


Figure 15. Reduction of standard deviation of FG departures of the microwave imagers. Standard deviations have been normalized by the value of the Control run and shown in percentage terms. (a) AMSR-E, (b) F17 SSMIS and (c) TMI from Test1. Panels (d–f) are the same but from Test2. White is the Northern Hemisphere, grey is the Tropics, and black is the Southern Hemisphere.

the microwave imagers in the Control run were reduced in Test1. The bias reduction in the Arabian Sea was remarkable. The bias reductions in the ascending and descending data in the Arabian Sea were approximately 0.6 and 0.7 K, respectively. Moreover, the biases in the northeast Pacific, southeast Pacific, and southeast Atlantic oceans were also reduced. The change in the Southern Hemisphere (close to 60°S and the southern extratropical storm track) were opposite between the ascending (negative) and the descending orbit (positive) because westerly winds were dominant in this area. Figure 12(c,d) show the impact of RWD model function changes for Metop-A AMSU-A channel 5 ascending and descending data, respectively. Figure 12(e,f) are Metop-A MHS channel 5. These are the lowest tropospheric microwave sounding channels for temperature and humidity respectively that are actively assimilated. Figure 12(c–f) does not show any surface-related geographical pattern either in ascending or descending data. Figure 13 shows the same comparisons but for AMSU-A surface-sensitive channels (channel 1, 2, 15). The impacts of RWD model changes were found as bias changes in low to moderate wind speed areas in the Tropics, especially in channel 2 (31.4 GHz). However, because the window channels

of the microwave sounding instruments are only used for cloud detection when assimilating the lower tropospheric channels in the ECMWF system, the differences of the assimilated data counts between the Test1 and Control runs were very small (e.g. approximately 0.05% difference for AMSU-A channel 5 and 0.01% difference for the MHS channel). The impacts of the RWD model function were minor for the assimilated microwave sounding data. However, major impacts were found for the microwave imager data. In other words, the impacts were found in surface-sensitive channels in the microwave frequency range from 19 to 89 GHz.

To confirm the relationship of the changes in the FG departure biases of the microwave imager channels and the surface wind field, the monthly mean 1000 hPa wind field for August 2011 from the analysis in Test1 is shown in Figure 14. In the experiment period (boreal summer), the strong south-westerly winds (Somali jet) in the Arabian Sea are clearly seen. The Somali jet is a high-wind-speed meteorological phenomenon with mean winds of more than 12 m s^{-1} from June to September every year. Moreover, this area is generally cloud-free in the boreal summer. The microwave imagers observe the surface directly without any

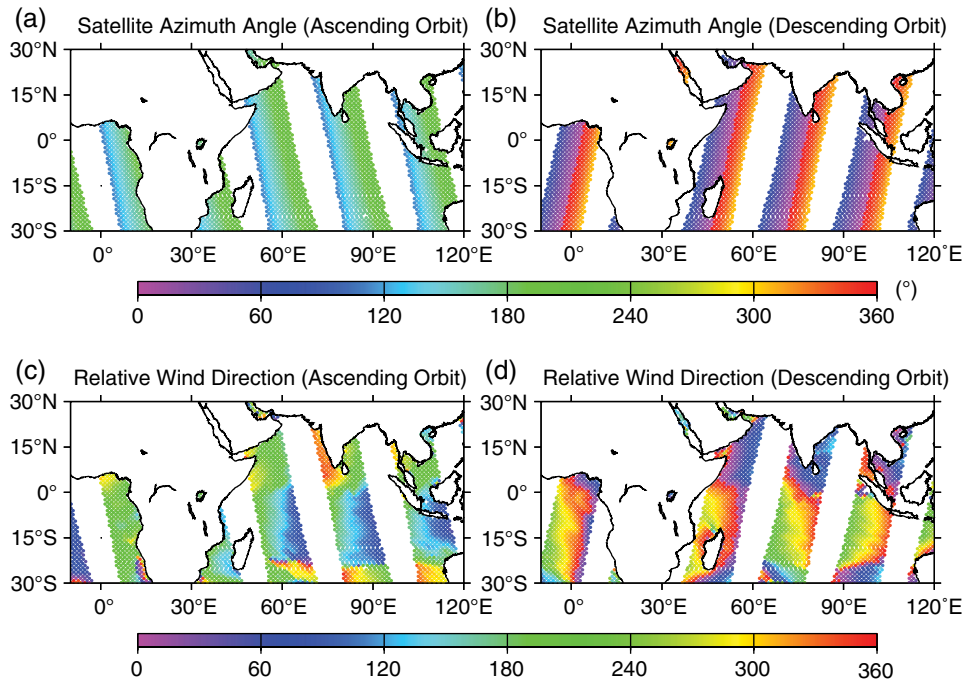


Figure 16. An example of AMSR-E satellite azimuth angle in the Arabian Sea. (a) Ascending orbit, (b) descending orbit. RWD distribution (c) ascending orbit, (d) descending orbit in the experiment. The units are degrees. An RWD of 0 or 360° corresponds to the upwind direction and 180° corresponds to the downwind direction.

cloud and rain contamination. The negatively biased area shown in Figure 11(a) has a good agreement with the high-wind area ($>10 \text{ m s}^{-1}$) in Figure 14. Moreover, other large difference areas in FG departure seen in Figure 12(a,b) correspond to areas with high wind-speed and low wind-direction variability.

Figure 15 shows reductions in the standard deviation of FG departures of the microwave imagers (AMSR-E, TMI and SSMIS) for three regions (Northern Hemisphere, Tropics and Southern Hemisphere). The standard deviations have been normalized by the value of the Control run and are shown in percentage terms. Panels (a), (b) and (c) are for Test1, and panels (d), (e) and (f) are for Test2. Generally, the global standard deviations of FG departures were reduced in Test1. The reduction of FG departures of vertically polarized channels in the Southern Hemisphere was significant. One reason for the larger impact is that high wind-speed areas occur more often in the Southern Hemisphere than in mid- and low- latitudes during the experiment period. The results in Test2 show less impact in the FG departure.

Figure 16 shows (a), (b) the satellite azimuth angle, and (c), (d) the relative wind direction for AMSR-E for the Arabian Sea. Although this is a single day in the experiment period, the pattern of the satellite azimuth angle and the RWD are similar during the period because conical scanning microwave imagers on polar-orbiting satellites observe the area with this fixed geometry every orbit. For the Arabian Sea, the value of RWD in ascending orbit (Figure 16(c)) is from 180 to 240° (downwind direction) and that in descending orbit (Figure 16(d)) is around 0 or 360° (upwind direction). The azimuthal variation in term of RWD has a minimum in the downwind direction (19V) and a maximum in the upwind direction as shown in Figure 2(a). The orbit-dependent biases shown in Figure 11 were caused by non-modelling of RWD variation in the Control run. In Test1, the biases caused by the azimuthal variation were reduced with the RWD model function in the radiative transfer calculations.

3.3. Impacts on atmospheric analysis and forecast

The microwave imager channels (19V, 19H, 23V, 23H, 37V and 89V) have strong sensitivity not only to surface wind but also to atmospheric humidity and cloud in the lower troposphere. The humidity information obtained from the microwave measurements plays an important role in the humidity

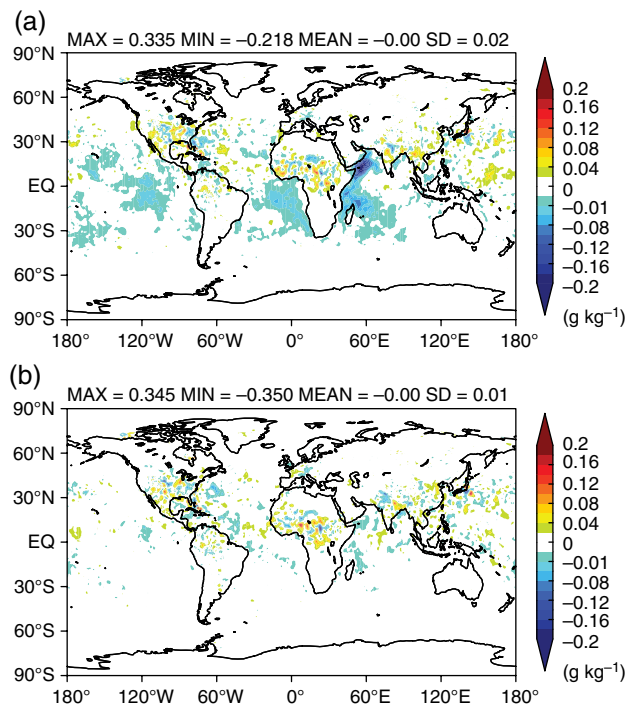


Figure 17. Mean RMS difference of 1000 hPa specific humidity analysis increment between the Test run and the Control run. (a) Test1, (b) Test2. Dark shading (blue in the online version) indicate a reduction in the analysis increment in the Test runs. The units are g kg^{-1} .

analysis and forecast. As most of the water vapour amounts are concentrated in the lower troposphere, we investigated mean difference of the RMS of analysis increments on the 1000 hPa specific humidity for Test1 (Figure 17(a)) and Test2 (Figure 17(b)). The largest reduction of the RMS of the analysis increment was found for the Arabian Sea (approximately 0.2 g kg^{-1}) in Test1. In the high-latitude areas in the Southern Hemisphere (along the storm track), the impact was small compared with other high-wind-speed areas. Although there are high-wind areas in the Southern Hemisphere, many microwave imager observations are not used because of large positive biases

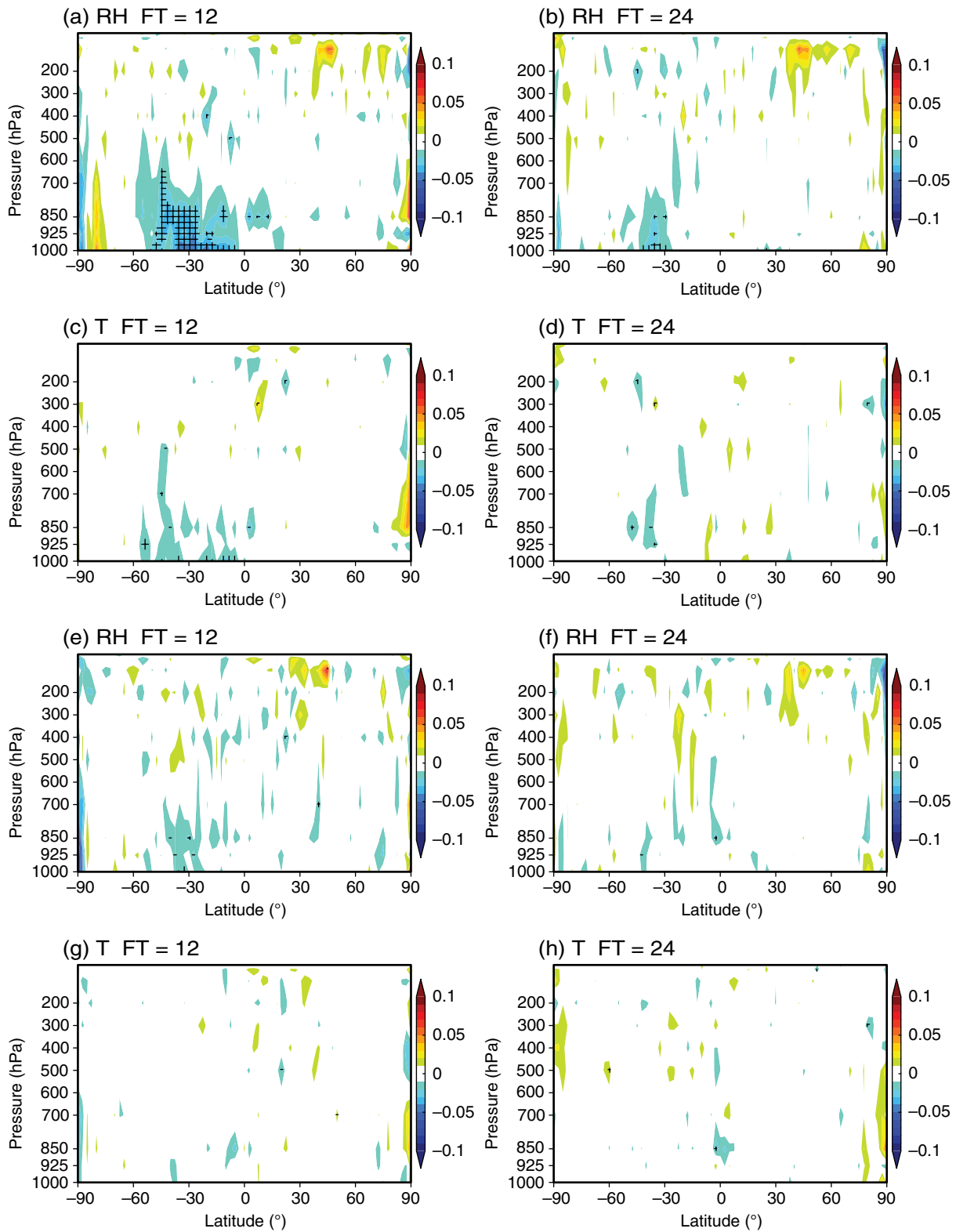


Figure 18. Normalized difference in relative humidity (RH) and temperature (T) forecast error (RMS) for 12 and 24 h forecasts. The top row is for relative humidity: (a) 12 h forecast, (b) 24 h forecast from Test1. Panels (c,d) are for temperature: (c) 12 h forecast, (d) 24 h forecast from Test1. Panels (e–h) are the same but from Test2. Cross-hatching indicates 95% statistical significance.

caused by a lack of cloud liquid water in cold sectors (Geer and Bauer, 2011) in the ECMWF forecast fields. The impacts on the analysis were small in the Test2 case.

The use of the RWD model function brought improvements in the forecast in Test1. Figure 18 shows normalized differences of RMS error of relative humidity (RH) and temperature (T) forecasts. The forecasts were verified against the experiment's own analysis. Blue colours indicate a reduction in the forecast error arising from the use of the RWD model function in the radiative transfer calculations. In the Southern Hemisphere lower troposphere, significant error reductions in RH and T were found

for short-range forecasts in Test1. The improvements of the RMS error at 12 h forecast indicate reductions of analysis increments of RH and T in the data assimilation. The impacts on the forecast were small in the Test2 case.

Figure 19 shows the normalized RMS error difference of RH as a function of forecast time for three pressure levels (500, 850 and 1000 hPa). Significant improvements were found in the Southern Hemisphere and the Tropics in the short-range forecasts for Test1 (solid circles). The results from Test2 are shown in open circles. The improvements in the Southern Hemisphere lower troposphere in Test1 were retained until day 3 of the forecast.

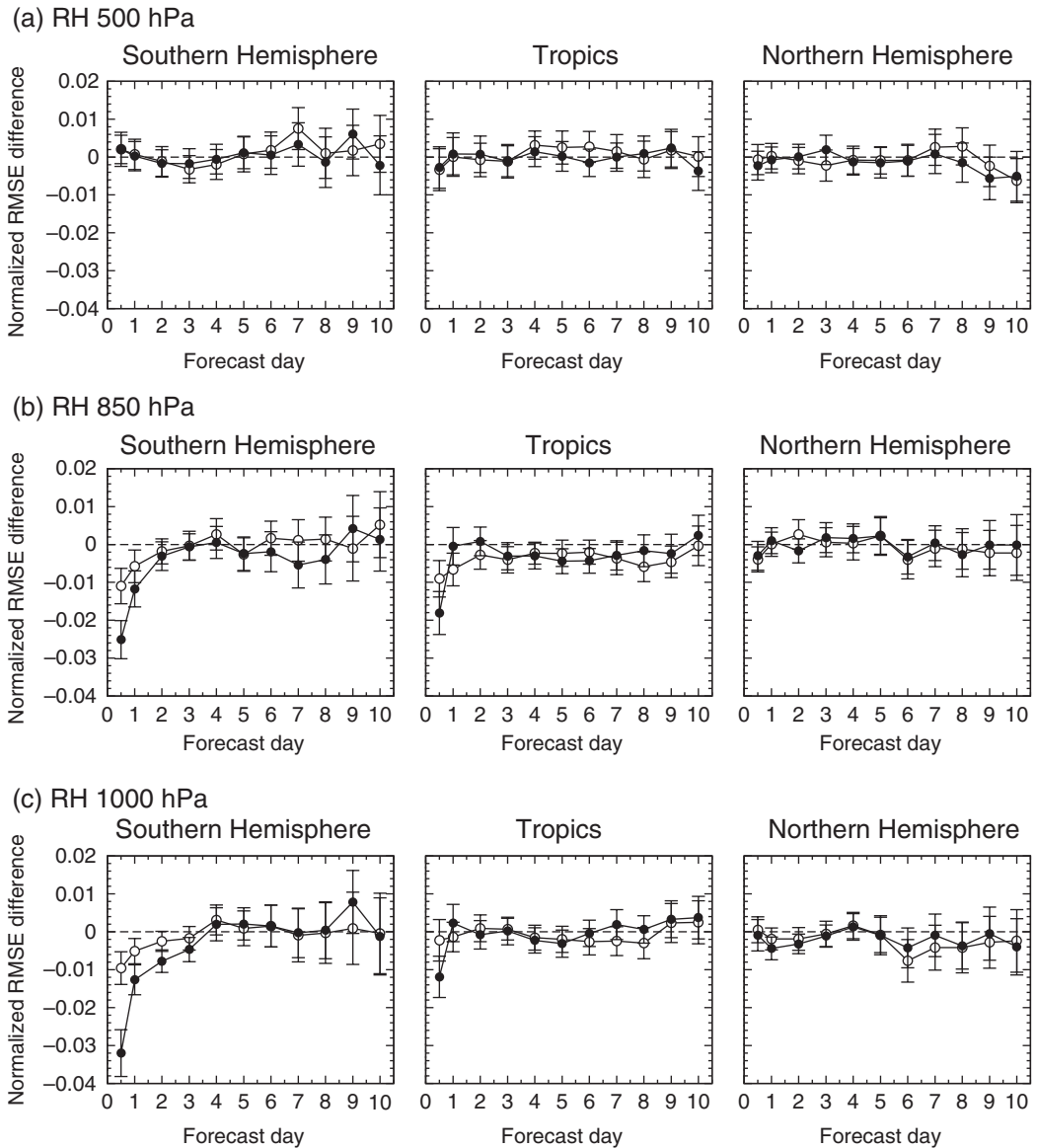


Figure 19. Normalized change in RMS forecast error in relative humidity at (a) 500 hPa, (b) 850 hPa, and (c) 1000 hPa for the Southern Hemisphere (latitudes -90 to -20), Tropics (latitudes -20 to 20), and Northern Hemisphere (latitudes 20 to 90). Verification is against own analysis. Scores are based on the experiment period 20 June to 3 October 2011. Error bars indicate the 95% confidence level. Solid circles are Test1 (the developed RWD model function), open circles are Test2 (FASTEM-5 azimuth model function).

Figure 20 is as Figure 19 but for temperature forecasts in the lower troposphere. Significant improvements of the temperature were found in the Southern Hemisphere and the Tropics in Test1. However, the improvements were limited in day 1 of the forecast. The results indicate the improvements in the short-range forecast could have been driven by the reductions of the humidity analysis increment in the data assimilation with our RWD model function.

4. Summary and conclusion

In this study, we focussed on the wind directional signals in the oceanic microwave radiance data. The azimuthal variation is a well-known phenomenon and many applications in remote sensing utilize it in geophysical product retrievals. However, the wind direction signals have not been actively taken into account in the radiative transfer calculation in data assimilation. ECMWF IFS FG fields do have sufficient accuracy to detect the azimuthal variation in the FG departure.

To utilize the wind direction signal in the data assimilation, a new Relative Wind Direction (RWD) model function was developed for the emissivity model. The development was based on simultaneous measurements of microwave radiance and surface wind vector from ADEOS-II AMSR and SeaWinds. Cloud-free conditions were selected to separate the surface signals

and the atmospheric signals in the observations. As for cloud-sensitive channels (89V and 89H), all-sky SSMIS data were used. The developed RWD model function was incorporated into the microwave ocean emissivity model (FASTEM-5) in RTTOV-10 for the impact study.

Input RWD was calculated from the surface wind vector in the FG field and the satellite azimuth angle. Because the satellite azimuth angles of SSMIS and TMI were not available in the real-time data in ECMWF IFS, the angles were calculated from the satellite position and the scan geometry in house. As the azimuth angle information is one of the basic satellite parameters for the radiative transfer calculation and other remote-sensing applications, the information should be included in the operational dataset by space agencies for future microwave imagers.

The RWD model function performances were different from those of FASTEM-5 (in RTTOV and CRTM) and FASTEM-3. In the experiments, the performance of our RWD model function brought reductions of the FG departure biases while FASTEM-5 azimuth model function brought smaller bias reductions than those of our RWD model function. It was difficult to reduce the bias in the RWD space by small amplitudes of FASTEM-5 azimuth model function in RTTOV, and the unphysical wind direction sensitivity at low wind-speed of FASTEM-5 and -3 could

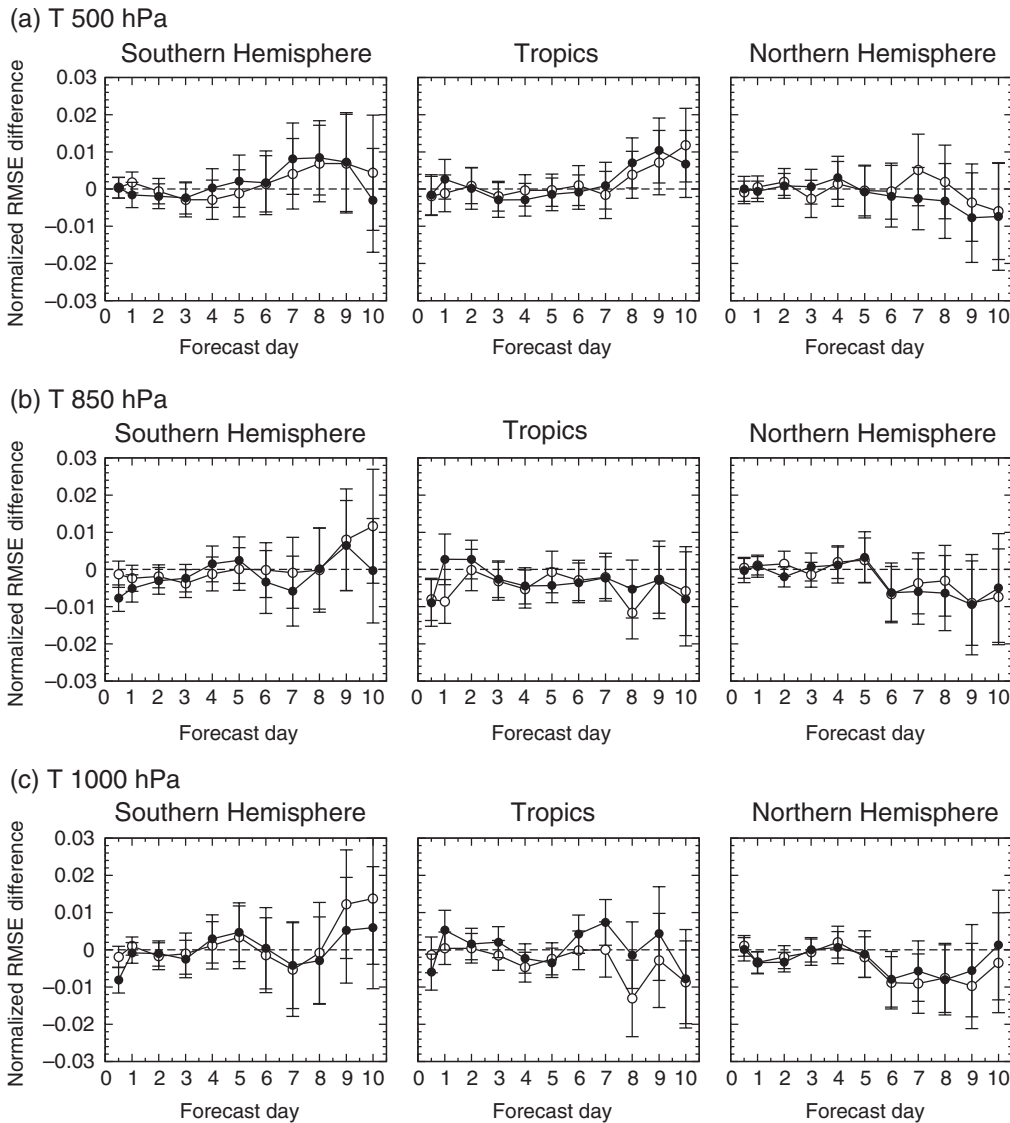


Figure 20. Same as Figure 19 but for temperature.

have negative impact. Because our RWD model function is based on real satellite measurements and less sensitivity at zero wind speed, it provided better performance than other models. This is confirmed in the comparison with real observations. The model function can be used for microwave imagers (e.g. AMSR-E, SSMIS and TMI) and temperature sounders (e.g. AMSU-A). The new RWD model function reduced the FG departure biases, especially in high wind speed and low wind direction variability areas (i.e. Arabian Sea, northeast Pacific, southeast Pacific, southeast Atlantic oceans) for the microwave imagers. The impacts for the microwave sounding channels for the assimilation were minor, but AMSU-A channel 2 (31.4 GHz) showed bias changes in low and moderate wind-speed areas.

The orbit-dependent biases of the microwave imagers in the Control run were caused by non-modelling of the azimuthal variation in the emissivity calculations. However, the experiment run using the new RWD function had lower biases. This is confirmed from the reduction of the analysis increment of the specific humidity at 1000 hPa. The changes in high wind-speed areas led to a significant improvement in RMS errors of the relative humidity and temperature fields in the lower troposphere for short-range forecasts.

The changes in FG departure using our new RWD model function were consistent with wind field and satellite azimuth angle relationships. Currently, the use of microwave imager radiance data in the Southern Hemisphere is limited due to cold sector biases (Geer and Bauer, 2011) in the ECMWF system. To enhance the use of the microwave imager data in the high-latitude

areas in future, the azimuthal variation should be treated with an accurate RWD model function in the radiative transfer model. The experiment results clearly showed the importance of the modelling of the azimuthal variation in the microwave radiance assimilation. The RWD model function should be in the radiative transfer model both for present microwave imagers and for upcoming new sensors, e.g. Global Change Observation Mission - Water1 (GCOM-W1) AMSR2 and the Global Precipitation Measurement Microwave Imager (GMI). The new RWD model function, combined with the other components of FASTEM-5, will be available as FASTEM-6 in RTTOV.

Acknowledgement

This study was carried out through a collaboration between ECMWF and the Japan Meteorological Agency (JMA). The authors acknowledge Alan Geer of ECMWF for his insightful comments and discussions. The authors would like to thank Akira Shibata of the Meteorological Satellite Center, JMA for providing the collocated ADEOS-II AMSR and SeaWinds data and valuable comments on this research topic. Takumu Egawa of JMA kindly provided the technical information on the satellite azimuth angle calculations. This work was funded by a Fellowship Program by the Ministry of Education, Culture, Sports, Science and Technology of the Japanese Government. This work was supported by Global Change Observation Mission - Water1 (GCOM-W1) research with Japan Aerospace Exploration Agency (JAXA) Earth Observation Research Center (EORC).

Appendix: Definition of relative wind direction

There are varying definitions used for the azimuthal wind and satellite angles. This appendix clarifies the situation, in particular the difference between FASTEM-5 and FASTEM-3, and it defines the angles used in the new relative wind direction (RWD) model function.

The satellite azimuth angle ϕ_s is defined using satellite location and observation location as Figure A1(a). The satellite azimuth angle is used as input for the radiative transfer calculation (RTTOV). In RTTOV, microwave ocean emissivity module (FASTEM) calculates the emissivity for each channel (vertical, horizontal polarization, and the third and the fourth Stokes parameters). The input satellite azimuth angle ϕ_s is passed to the FASTEM. Azimuthal angle information used in FASTEM is calculated from the satellite azimuth angle ϕ_s and surface wind direction (10 m wind direction from NWP FG field). The definition of the azimuthal angle information is different between FASTEM-5 and FASTEM-3. FASTEM-4 azimuthal model function is the same as FASTEM-5 azimuthal function.

As shown in Figure A1(a), the satellite azimuth angle ϕ_s and satellite azimuth view (looking) angle ϕ_v are related as follows:

$$\phi_v = \phi_s + 180. \quad (\text{A1})$$

The angles are measured clockwise from north and describe a 0 to 360° range as shown in Figure A1(a).

In FASTEM, the 10 m wind direction ϕ_w is defined as a direction towards which the wind is blowing. In meteorological

convention, wind direction ϕ_m is defined as a direction from which the wind is blowing (Figure A1(b)). The FASTEM wind direction ϕ_w and the meteorological wind direction ϕ_m are related as follows:

$$\phi_m = \phi_w + 180. \quad (\text{A2})$$

The wind directions are measured clockwise from north and describe a 0 to 360° range.

FASTEM-5 uses RWD as input azimuthal angle information. RWD ϕ_r is defined as wind direction relative to the satellite azimuth angle. RWD is defined as follows:

$$\phi_r = \phi_w - \phi_s, \quad (\text{A3})$$

where ϕ_w is FASTEM wind direction and ϕ_s is the satellite azimuth angle. Our RWD model function uses ϕ_r as input azimuthal angle information. The ranges of ϕ_w and ϕ_s are from 0 to 360° . RWD ϕ_r describes a $0-360^\circ$ range. Using Eqs (A1), (A2) and (A3) it can be written as follows:

$$\phi_r = \phi_m - \phi_v. \quad (\text{A4})$$

Equation (A4) indicates that RWD can be calculated from the meteorological wind direction and the satellite azimuth view angle. Figure A1(c) illustrates the definition of RWD ϕ_r in a westerly wind case using the FASTEM wind direction ϕ_w and the satellite azimuth angle ϕ_s .

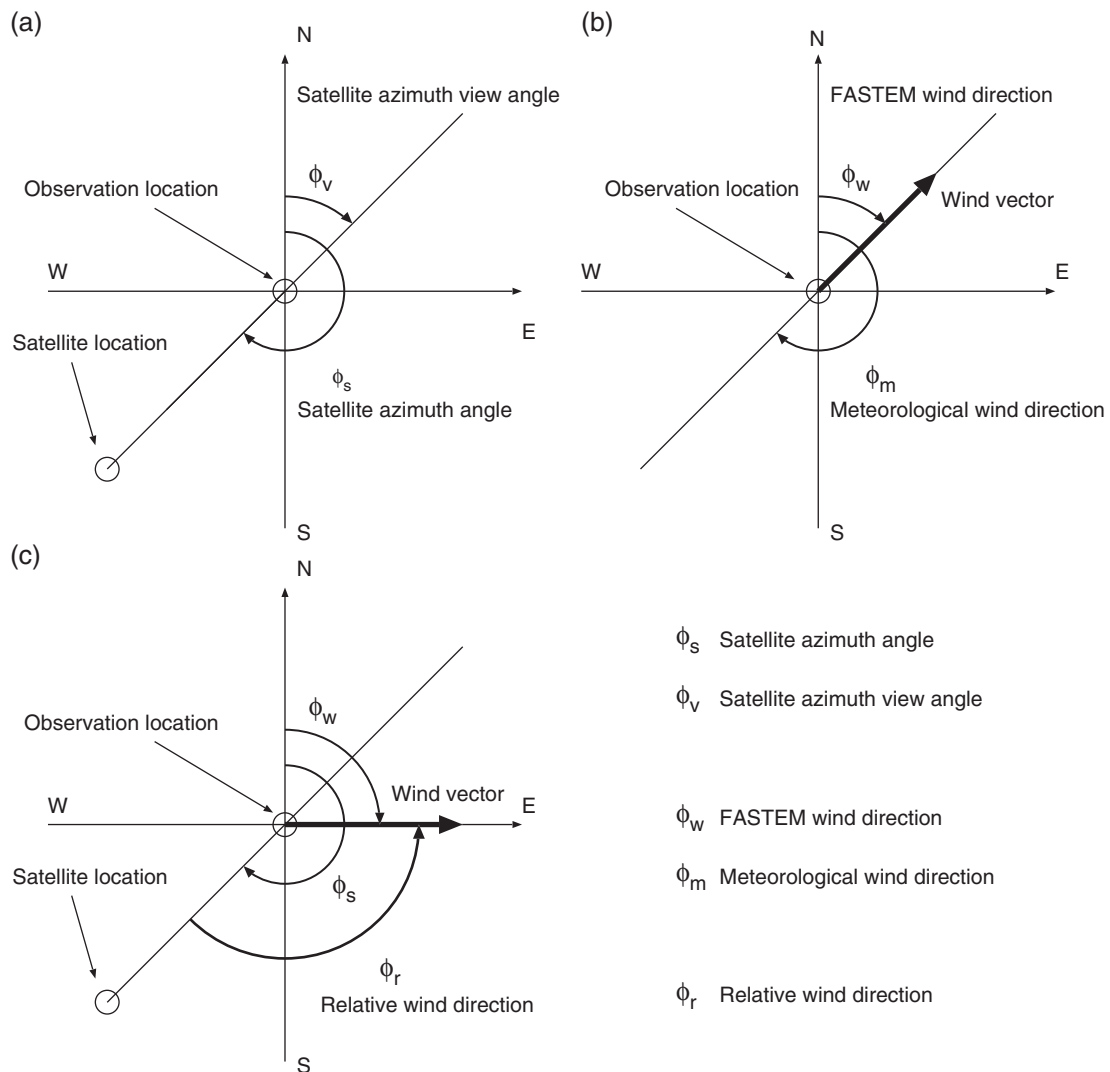


Figure A1. Definitions of angles. (a) Satellite azimuth view angle and Satellite azimuth angle. (b) FASTEM wind direction and Meteorological wind direction. (c) Relative wind direction (westerly wind case). Wind vector is drawn as thick black arrow.

On the other hand, FASTEM-3 uses azimuth line of sight less the wind direction (Saunders *et al.*, 2006) as the azimuthal angle information. The angle $\phi_{r(\text{FASTEM-3})}$ is defined as follows:

$$\phi_{r(\text{FASTEM-3})} = \phi_s - \phi_w. \quad (\text{A5})$$

However, in the coding of RTTOV-10, actual input is defined as follows:

$$\phi_{r(\text{FASTEM-3})} = 180 - (\phi_w - \phi_s). \quad (\text{A6})$$

By using Eqs (A1) and (A6) it can be written as follows:

$$\phi_{r(\text{FASTEM-3})} = \phi_v - \phi_w. \quad (\text{A7})$$

Equation (A7) implies that FASTEM-3 azimuthal model function in RTTOV uses satellite azimuth view angle ϕ_v . This is an inconsistency in the present RTTOV coding and FASTEM-3 definition. In this study, we use the correct input for the azimuthal variation calculation for FASTEM-3 (results shown in Figure 7).

References

- Bauer P, Geer AJ, Lopez P, Salmond D. 2010. Direct 4D-Var assimilation of all-sky radiances. Part I: Implementation. *Q. J. R. Meteorol. Soc.* **136**: 1868–1885, doi: 10.1002/qj.659.
- Bauer P, Beljaars A, Ahlgren M, Bechtold P, Bidlot JR, Bonavita M, Bozzo A, Forbes R, Hólm E, Leutbecher M, Lopez P, Magnusson L, Prates F, Rodwell M, Sandu I, Untch A, Vitart F. 2013. *Model Cycle 38r2: Components and Performance, ECMWF Technical Memorandum 704*. ECMWF: Reading, UK. <http://www.ecmwf.int> (accessed 15 June 2014).
- Bormann N, Geer AJ, Wilhelmsen T. 2011. *Operational Implementation of RTTOV-10 in the IFS, ECMWF Technical Memorandum 650*. ECMWF: Reading, UK. <http://www.ecmwf.int> (accessed 15 June 2014).
- Bormann N, Geer AJ, English SJ. 2012. *Evaluation of the Microwave Ocean Surface Emissivity Model FASTEM-5 in the IFS, ECMWF Technical Memorandum 667*. ECMWF: Reading, UK. <http://www.ecmwf.int> (accessed 15 June 2014).
- Deblonde G, English SJ. 2001. ‘Evaluation of the FASTEM2 fast microwave oceanic surface emissivity model’. In *Technical Proceedings of International TOVS Working Group-XI*, 20–26 September 2000, Budapest.
- Dee D. 2004. Variational bias correction of radiance data in the ECMWF system. In *Proceedings of Workshop on Assimilation of High Spectral Resolution Sounders in NWP*, 28 June–1 July 2004. ECMWF: Reading, UK. <http://www.ecmwf.int> (accessed 15 June 2014).
- Dee DP, Uppala SM, Simmons AJ, Berrisford P, Poli P, Kobayashi S, Andrae U, Balmaseda MA, Balsamo G, Bauer P, Bechtold P, Beljaars ACM, van de Berg L, Bidlot J, Bormann N, Delsol C, Dragani R, Fuentes M, Geer AJ, Haimberger L, Healy SB, Hersbach H, Hólm EV, Isaksen L, Källberg P, Köhler M, Matricardi M, McNally AP, Monge-Sanz BM, Morcrette J-J, Park B-K, Peubey C, de Rosnay P, Tavolato C, Thépaut J-N, Vitart F. 2011. The ERA-Interim reanalysis: Configuration and performance of the data assimilation system. *Q. J. R. Meteorol. Soc.* **137**: 553–597, doi: 10.1002/qj.828.
- Dzura MS, Etkin VS, Khrupin AS, Pospelov MN, Raev MD. 1992. ‘Radiometers-polarimeters: Principles of design and applications for sea surface microwave emission polarimetry’. In *Proceedings of the 1992 IEEE International Geoscience and Remote Sensing Society (IGARSS)*, 26–29 May 1992, Houston, TX, doi: 10.1109/IGARSS.1992.578475.
- Ebuchi N. 2006. Evaluation of marine surface winds observed by seawinds and AMSR on ADEOS-II. *J. Oceanogr.* **62**: 293–301, doi: 10.1007/s10872-006-0054-6.
- English SJ, Hewison TJ. 1998. A fast generic millimetre-wave emissivity model. *Proc. SPIE* **3503**: 288–300.
- Etkin VS, Raev MD, Bulatov MG, Militsky YA, Smirnov AV, Raizer VY, Trokhimovsky YA, Irisov VG, Kuzmin AV, Litovchenko KT, Bespalova EA, Skvortsov EI, Pospelov MN, Smirnov AI. 1991. ‘Radiohydrophysical aerospace research of ocean’, Technical Report IIp-1749. Academy of Science, Space Research Institute: Moscow.
- Geer AJ, Bauer P. 2011. Observation errors in all-sky data assimilation. *Q. J. R. Meteorol. Soc.* **137**: 2024–2037, doi: 10.1002/qj.830.
- Geer AJ, Bauer P, Lopez P. 2010. Direct 4D-Var assimilation of all-sky radiances. Part II: Assessment. *Q. J. R. Meteorol. Soc.* **136**: 1886–1905, doi: 10.1002/qj.681.
- Janssen MA. (ed.) 1993. *Atmospheric Remote Sensing by Microwave Radiometry*. John Wiley & Sons, Inc.: New York, NY.
- Kawanishi T, Sezai T, Ito Y, Imaoka K, Takeshima T, Ishido Y, Shibata A, Miura M, Inahata H, Spencer RW. 2003. The advanced microwave scanning radiometer for the Earth observing system (AMSR-E), NASA’s contribution to the EOS for global energy and water cycle studies. *IEEE Trans. Geosci. Remote Sens.* **41**: 184–194, doi: 10.1109/TGRS.2002.808331.
- Kumabe R, Egawa T. 2011. ‘Development of a procedure to make better use of SSM/I data including navigation errors’, Meteorological Satellite Center Technical Note 55. Japan Meteorological Agency: Tokyo.
- Liou KN. 2002. *An Introduction to Atmospheric Radiation* (2nd edn). Academic Press: San Diego, CA.
- Liu Q, Weng F. 2003. Retrieval of sea surface wind vector from simulated satellite microwave polarimetric measurements. *Radio Sci.* **38**: 8078, doi: 10.1029/2002RS002729.
- Liu Q, Weng F, English SJ. 2011. An improved fast microwave water emissivity model. *IEEE Trans. Geosci. Remote Sens.* **49**: 1238–1250, doi: 10.1109/TGRS.2010.2064779.
- Meissner T, Wentz F. 2002. An updated analysis of the ocean surface wind direction signal in passive microwave brightness temperatures. *IEEE Trans. Geosci. Remote Sens.* **40**: 1230–1240, doi: 10.1109/TGRS.2002.800231.
- Meissner T, Wentz FJ. 2012. The emissivity of the ocean surface between 6 and 90 GHz over a large range of wind speeds and Earth incidence angles. *IEEE Trans. Geosci. Remote Sens.* **50**: 3004–3026, doi: 10.1109/TGRS.2011.2179662.
- Monahan EC, O’Muircheartaigh IG. 1986. Whitecaps and the passive remote sensing of the ocean surface. *Int. J. Remote Sens.* **7**: 627–642.
- St. Germain KM, Poe GA, Gaiser PW. 2002. Polarimetric Emission Model of the Sea at Microwave Frequencies and Comparison with Measurements. *Prog. Electromag. Res.* **37**: 1–30.
- Saunders R, Matricardi M, Brunel P. 1999. An improved fast radiative transfer model for assimilation of satellite radiance observations. *Q. J. R. Meteorol. Soc.* **125**: 1407–1425, doi: 10.1002/qj.1999.49712555615.
- Saunders R, Andersson E, Brunel P, Chevallier F, Deblonde G, English SJ, Matricardi M, Rayer P, Sherlock V. 2002. ‘RTTOV-7 – Science and validation report’, v1.3. EUMETSAT NWP-SAF.
- Saunders R, Brunel P, English SJ, Bauer P, O’Keeffe U, Francis P, Rayer P. 2006. ‘RTTOV-8 – Science and validation report’, NWPSAF-MO-TV-007, v1.6. EUMETSAT NWP-SAF.
- Saunders R, Hocking J, Rayer P, Matricardi M, Geer A, Bormann N, Brunel P, Karbou F, Aires F. 2012. ‘RTTOV-10 science and validation report’, NWPSAF-MO-TV-023, v1.11. EUMETSAT NWP-SAF.
- Saunders R, Hocking J, Rundle D, Rayer P, Matricardi M, Geer A, Lupu C, Brunel P, Vidot J. 2013. ‘RTTOV-11 science and validation report’, NWPSAF-MO-TV-032, v1.11. EUMETSAT NWP-SAF.
- Tang C. 1974. The effect of droplets in the air-sea transition zone on the sea brightness temperature. *J. Phys. Oceanogr.* **4**: 579–593.
- Tsang L. 1991. Polarimetric passive microwave remote sensing of random discrete scatterers and rough surfaces. *J. Electromagn. Waves Appl.* **5**: 41–57.
- Weng F, Han Y, van Delst P, Liu Q, Yan B. 2005. ‘JCSDA community radiative transfer model (CRTM)’. In *Technical Proceedings of International TOVS Working Group-XIV*, 25–31 May 2005, Beijing.
- Wentz FJ. 1992. Measurement of oceanic wind vector using satellite microwave radiometers. *IEEE Trans. Geosci. Remote Sens.* **30**: 960–972.
- Wentz FJ. 1997. A well-calibrated ocean algorithm for special sensor microwave/imager. *J. Geophys. Res.* **102**: 8703–8718, doi: 10.1029/96JC01751.
- Yueh SH. 1997. Modeling of wind direction signals in polarimetric sea surface brightness temperatures. *IEEE Trans. Geosci. Remote Sens.* **35**: 1400–1418.
- Yueh SH, Kwok R, Li FK, Nghiem SV, Wilson WJ. 1994. Polarimetric passive remote sensing of ocean wind vectors. *Radio Sci.* **29**: 799–814.
- Yueh SH, Wilson WJ, Li FK, Nghiem SV, Ricketts WB. 1995. Polarimetric measurements of sea surface brightness temperatures using an aircraft K-band radiometer. *IEEE Trans. Geosci. Remote Sens.* **33**: 85–92.
- Yueh SH, Wilson WJ, Li FK, Nghiem SV, Ricketts WB. 1997. Polarimetric brightness temperatures of sea surfaces measured with aircraft K- and Ka-band radiometers. *IEEE Trans. Geosci. Remote Sens.* **35**: 1177–1187.
- Yueh SH, Wilson WJ, Dinardo SJ, Li FK. 1999. Polarimetric microwave brightness signatures of ocean wind directions. *IEEE Trans. Geosci. Remote Sens.* **37**: 949–959.